



Interdecadal change in the relationship between boreal winter North Pacific Oscillation and Eastern Australian rainfall in the following autumn

Linye Song¹ · Shangfeng Chen² · Wen Chen^{2,3} · Wansuo Duan³ · Yun Li⁴

Received: 18 January 2021 / Accepted: 23 June 2021

© The Author(s), under exclusive licence to Springer-Verlag GmbH Germany, part of Springer Nature 2021

Abstract

Previous study reported that boreal winter North Pacific Oscillation (NPO) has a pronounced impact on the interannual variation of eastern Australian rainfall in the following autumn. This study reveals that impact of the winter NPO on the eastern Australian rainfall shows a marked interdecadal weakening around the late-1990s. Before the late-1990s, winter NPO leads to warm sea surface temperature anomalies (SSTAs) in the subtropical North Pacific during succedent spring via modulating surface heat fluxes. Warm SSTAs enhance atmospheric heating and lead to westerly wind anomalies over the tropical western-central Pacific via wind-evaporation-SST feedback process. The westerly wind anomalies over the tropical western-central Pacific contribute to an El Niño-like pattern in the following autumn, which further leads to decrease in the eastern Australian rainfall via modulating the tropical Walker circulation. However, after the late-1990s, winter NPO-related atmospheric anomaly shifts northward compared to that before the late-1990s. As such, the NPO-generated spring SSTAs over the subtropical North Pacific, and the westerly wind anomalies over the tropical western-central Pacific are much weaker. Hence, winter NPO cannot induce a clear El Niño-like pattern in the following autumn, and thus cannot impact eastern Australian rainfall after the late-1990s. Northward displacement of the winter NPO-related atmospheric anomalies after the late-1990s is due to northward movement of the climatological mean circulation and storm track over North Pacific. Further analysis indicates that Atlantic Multidecadal Oscillation (AMO) has a strong influence on the meridional movement of the NPO via modulating North Pacific climatological mean circulation. We suggest that AMO acts as a crucial modulator for the relation between winter NPO and subsequent autumn Australian rainfall.

Keywords North Pacific Oscillation · Rainfall · Australia · Sea surface temperature · Walker circulation · Interdecadal change · Atlantic Multidecadal Oscillation

1 Introduction

Australia is one of the most important agricultural producers in the world. Agriculture and associated sectors in Australia earn about \$155 billion per year for a 12% share of the gross domestic product (<http://www.nff.org.au/farm-facts.html>). In addition, it is known that Australia is one of the driest continents in the world, with a climate featured by large variations of rainfall both on the interannual and interdecadal timescales (Gallant et al. 2007). Therefore, one major issue facing agriculture in Australia is drought event, which could lead to large challenges to water availability for agriculture and result in severe loss of social economy. For instance, eastern part of Australia underwent a serious drought event in 2002–2003, which led to 25% decrease of gross farm product in Australia (Lu and Hedley 2004).

Shangfeng Chen
chenshangfeng@mail.iap.ac.cn

¹ Institute of Urban Meteorology, China Meteorological Administration, Beijing, China

² Center for Monsoon System Research, Institute of Atmospheric Physics, Chinese Academy of Sciences, Beijing, China

³ State Key Laboratory of Numerical Modeling for Atmospheric Sciences and Geophysical Fluid Dynamics, Institute of Atmospheric Physics, Chinese Academy of Sciences, Beijing, China

⁴ Business Intelligence and Data Analytics, Western Power, Perth, WA 6000, Australia

Serious drought events in Australia in the past were usually related to decrease in the rainfall in boreal autumn (September–October–November, corresponding to austral spring) (BOM 2006; Song et al. 2016). For instance, decrease in the rainfall in boreal summer and autumn of 2006 in Australia leads to annual rainfall of 2006 being about 50% below normal over most parts of Australia. By contrast, the recorded wettest autumn in 2010 in eastern part of Australia had largely relieved the long-term drought conditions since 1995. Hence, it is of great importance to improve our understanding of rainfall variation in Australia and the associated physical processes.

Previous studies indicated that autumn rainfall variation in Australia can be impacted by many factors, including sea surface temperature (SST) anomalies off the northern coast of Australia (Nicholls 1984a, 2010; Ummenhofer et al. 2008; Catto et al. 2012), SST anomalies related to the El Niño-Southern Oscillation (ENSO) (Nicholls 1984b; Ropelewski and Halpert 1987; Chiew et al. 1998; Cai and Cowan 2009; Taschetto and England 2009; Cai et al. 2010), SST anomalies related to the Indian Ocean dipole (IOD) (Saji et al. 1999; Ashok et al. 2003; Cai et al. 2009; Ummenhofer et al. 2011). For instance, studies indicated that SST anomalies related to the El Niño (La Niña) event tend to lead to decrease (increase) in the rainfall over most parts of eastern Australia in boreal autumn via modulating the tropical walker circulation (Allan 1988; Chiew et al. 1998; Wang and Hendon 2007; Cai and Cowan 2009). In addition to the tropical forcings, studies reported that atmospheric variability over extratropical regions can exert significant impacts on the Australian rainfall. For example, Hendon et al. (2007) reported that Southern Hemisphere annual mode (SAM) (also called Antarctic Oscillation) has a close relation with the rainfall over Australia. In particular, positive phase of the SAM in winter would lead to decrease in rainfall over southeast and southwest Australia. Hendon et al. (2007) showed that SAM explains about 15% of the weekly rainfall in the above regions, comparable to that explained by the ENSO. SAM is the dominant mode of the atmospheric variability on the interannual timescale over extratropical southern Hemisphere, which can not only exert substantial impacts on weather and climate variations over southern Hemisphere, but also over northern Hemisphere (e.g., Wu et al. 2009, 2015; Dou et al. 2017, 2020; Dou and Wu 2018). Zhu and Wang (2010) showed that change in the intensity of Aleutian Low in boreal winter has a notable impact on the Australian summer monsoon and precipitation over Australia via atmospheric teleconnection.

A recent study of Song et al. (2016) indicated that the North Pacific Oscillation (NPO; Walker and Bliss 1932; Linkin and Nigam 2008) in boreal winter has a significant impact on the rainfall variation over eastern Australia in boreal autumn of next year. NPO is one of the most

important atmospheric teleconnection patterns over Northern Hemisphere (Linkin and Nigam 2008). Song et al. (2016) suggested that winter NPO firstly leads to an ENSO-like SST anomaly pattern in the following autumn via the seasonal footprinting mechanism proposed by Vimont et al. (2001, 2003a, b). Then, the autumn ENSO-like SST anomalies generated by preceding winter NPO further impact rainfall over Australia via modulating the tropical walker circulation (Song et al. 2016).

Previous studies indicated that connection of the winter NPO with the following ENSO has experienced significant interdecadal changes in the past (Yu et al. 2012; Yeh et al. 2018; Chen et al. 2019a, b). As ENSO plays a key role in relaying the impact of the winter NPO on the following rainfall variation over Australia, it is reasonable to speculate that the NPO-Australian rainfall relation may have changed in the past. Investigating the stability of the connection between the winter NPO and following autumn Australian rainfall variation is of great importance to the prediction of the Australian rainfall based on the preceding winter NPO. In this study, we present observational evidences to show that connection of the winter NPO with the Australian rainfall in the following autumn experienced a significant interdecadal change around the late-1990s. We will also examine the factors responsible for this interdecadal change.

The structure of this paper is organized as follows. Section 2 describes the data and methods used in this study. Section 3 examines interdecadal change in the relationship between winter NPO and Australian rainfall. Section 4 investigates the factors contributing to change in the impact of winter NPO on the rainfall over Australia. Section 5 discusses possible role of the AMO in modulating the winter NPO-Australian rainfall relation. Section 6 provides a summary.

2 Data and methods

Monthly and daily mean sea level pressure (SLP), horizontal winds, geopotential height, surface latent and sensible heat fluxes, and surface net shortwave and longwave radiations used in this study are extracted from the National Centers for Environmental Prediction (NCEP)-National Center for Atmospheric Research (NCAR) reanalysis dataset (Kalnay 1996; <ftp://ftp.cdc.noaa.gov/Datasets/>), which is available from January 1948 to the present. Atmospheric data of the NCEP-NCAR reanalysis have a horizontal resolution of $2.5^\circ \times 2.5^\circ$ and extend from 1000-hPa to 100-hPa with 17 pressure levels. Surface heat fluxes are derived from the NCEP-NCAR reanalysis on T62 Gaussian grids. We also employ the atmospheric data from the European Centre for Medium-Range Weather Forecasts interim reanalysis (ERA-Interim) (Dee et al. 2011), and Japanese 55-Year reanalysis

(JRA55) (Ebita et al. 2011) to confirm the results obtained from the NCEP-NCAR reanalysis. The ERA-Interim reanalysis data are available from January 1979 to August 2019, and the JRA55 reanalysis data cover the period from January 1958 to the present. Results obtained from the above three reanalysis datasets are highly similar. Thus, we only present those obtained from the NCEP-NCAR reanalysis unless otherwise stated.

This study also employs the monthly mean SST data from the National Oceanic and Atmospheric Administration Extended Reconstructed SST version 5 (NOAA-ERSSTV5) (Huang 2017; <https://www.esrl.noaa.gov/psd/data/gridded/>), which is available from January 1854 to the present with a horizontal resolution of $2^\circ \times 2^\circ$. Monthly mean rainfall data over land area are obtained from the University of Delaware surface air temperature and precipitation dataset version v5.01 (Matsuura and Willmott 2009; https://www.esrl.noaa.gov/psd/data/gridded/data.UDel_AirT_Precip.html). This dataset has a horizontal resolution of $0.5^\circ \times 0.5^\circ$ and covers the period from January 1900 to December 2017. In addition, monthly mean rainfall data over oceanic region are derived from the Global Precipitation Climatology Project (GPCP) spanning from 1979 to the present with a horizontal resolution of $2.5^\circ \times 2.5^\circ$ (Adler et al. 2003; <http://www.esrl.noaa.gov/psd/data/gridded/data.gpcp.html>). Furthermore, this study uses the monthly mean AMO index from the Physical Science Division of NOAA from 1948 to the present (<https://www.esrl.noaa.gov/psd/data/timeseries/AMO/>).

Synoptic-scale eddies activity (also called storm track) is represented by the root-mean-square of the 2–8-day band-pass filtered geopotential height anomalies as in previous studies (Chen et al. 2014, 2018a). In addition, following Song et al. (2016), the NPO index is defined as difference in the normalized SLP anomalies over mid-latitude North Pacific ($45^\circ\text{--}70^\circ\text{ N}$, $125^\circ\text{--}175^\circ\text{ W}$) and subtropical North Pacific ($10^\circ\text{--}25^\circ\text{ N}$, $175^\circ\text{ E}\text{--}145^\circ\text{ W}$). The Niño-3.4 SST index is used to represent the ENSO variability, which is defined as region-mean SST anomalies over $5^\circ\text{ S}\text{--}5^\circ\text{ N}$ and $120^\circ\text{--}170^\circ\text{ W}$. In this study, we concentrate on examining interannual relationship between wintertime NPO and rainfall variation over Australia in the following autumn. Thus, all the variables are subjected to a 2–9 Lanczos band-pass filter to extract their interannual components (Duchon 1979). Interannual component of rainfall anomalies in autumn accounts for above 70% of the total rainfall variability over most parts of Australia, with the largest value reaching above 85% over coastal regions (Fig. 1a). To ensure that the significant connection of the winter NPO with the following autumn Australian rainfall analyzed in this study is not due to the ENSO cycle, following Vimont et al. (2003a, b) and Zhao et al. (2019a, b, 2020), we have removed the winter ENSO signal from the winter NPO index as follows:

$$\text{NPO}_{\text{res}} = \text{NPO} - \text{RC} \times \text{Niño} - 3.4.$$

Here, NPO indicates winter NPO index and Niño-3.4 denotes the simultaneous winter Niño-3.4 SST index. RC is the regression coefficient between the winter Niño3.4 index and the winter NPO index. NPO_{res} is the part of the winter NPO index that winter ENSO signal has been removed.

Significance levels of correlation coefficients and regression coefficients are estimated by the two-tailed Student's *t* test. Since auto-correlation may exist for the band-pass filtered time series, we calculate the effective degree of freedom (EDOF) according to the method proposed by Bretherton et al. (1999), which is expressed as follows:

$$\text{EDOF} = N \times \frac{1 - r_1 r_2}{1 + r_1 r_2} - 2$$

Here, r_1 and r_2 denote the lag-one auto-correlation coefficients of the two time series employed to the correlation and regression analyses. N is the sample size of the original time series.

We use the Fisher's *r*-*z* transformation technique to identify the significance level of the difference between two correlation coefficients (CC_1 and CC_2). Correlation coefficients CC_1 and CC_2 are firstly transformed by the following equations:

$$Z_1 = \frac{1}{2} \cdot \ln \left[\frac{1 + CC_1}{1 - CC_1} \right],$$

$$Z_2 = \frac{1}{2} \cdot \ln \left[\frac{1 + CC_2}{1 - CC_2} \right].$$

Then, standard parametric test is employed to estimate the null hypothesis of the equality of Z_1 and Z_2 . The test statistic (U) is written as follows:

$$U = \frac{Z_1 - Z_2}{\sqrt{\frac{1}{N_1-3} + \frac{1}{N_2-3}}}$$

where, N_1 (N_2) denotes sample size of the time series used to calculate the CC_1 (CC_2). Statistic U is normally distributed. Thus, the statistical significance level is evaluated based on the two-tailed Student's *t* test.

3 Change in the relation between boreal winter NPO and Australian rainfall

Spatial pattern of the boreal winter (ND(−1)JFM(0)) NPO is shown in Fig. 2a, which is represented by winter SLP anomalies regressed upon the simultaneous winter NPO index. Time notations of “−1” and “0” denote the years before and during the rainfall variation over Australia,

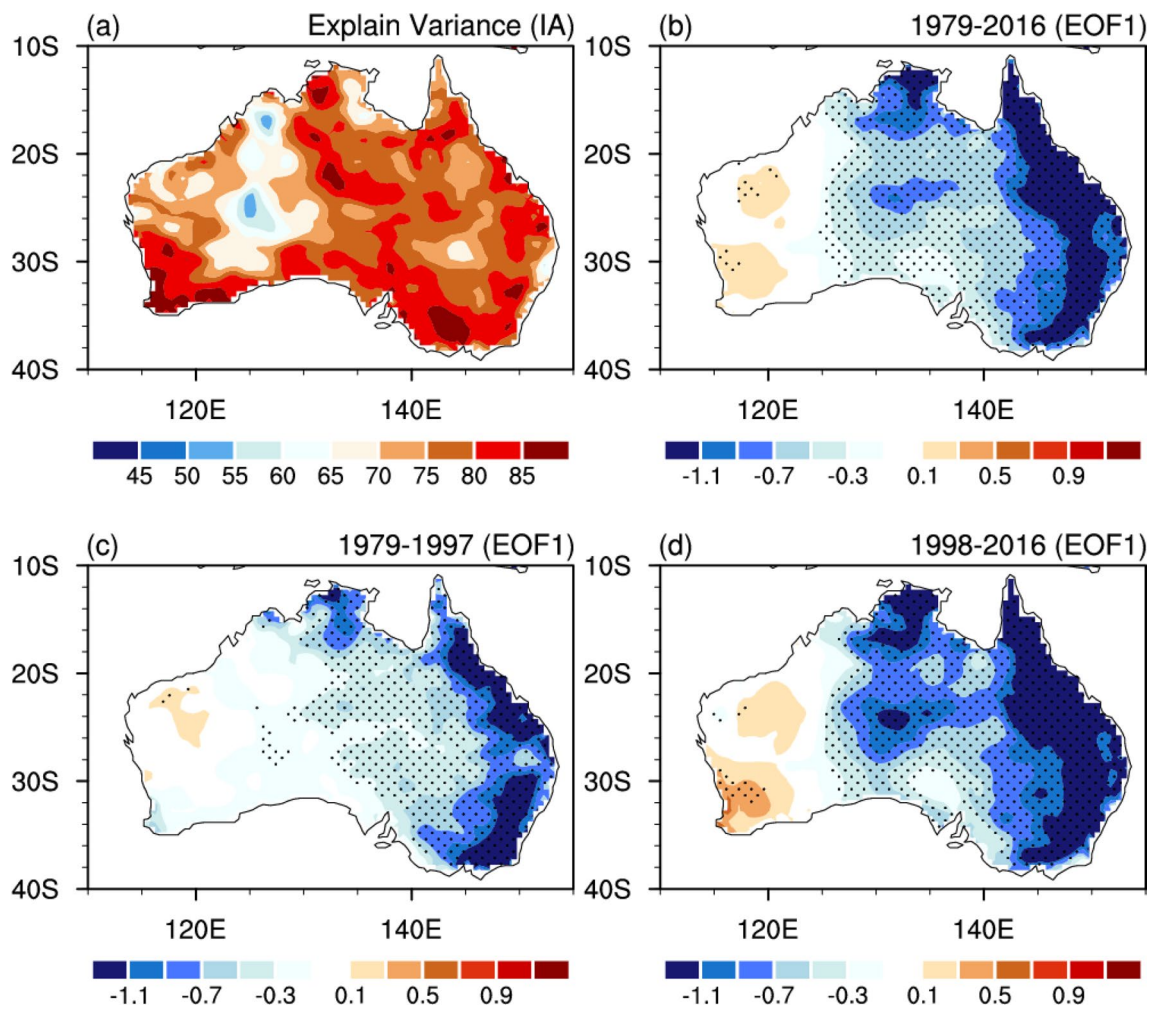


Fig. 1 **a** Variance fraction (unit: %) of original rainfall anomalies in SON(0) over Australia explained by its interannual component for the period of 1979–2016. Rainfall anomalies (unit: cm) in SON(0) over Australia obtained by regression upon the PC time series correspond-

ing to the EOF1 of Australian Rainfall anomalies in SON(0) for the period of **b** 1979–2016, **c** 1979–1997, and **d** 1998–2016, respectively. Stippling regions in—**b–d** indicate rainfall anomalies significant at the 95% confidence level

respectively. Note that the season described in the following corresponds to that in the Northern Hemisphere unless otherwise stated. For example, autumn denotes the mean of September, October and November (SON for short), and spring represents the average of March, April, and May (MAM for short). During positive phase of the winter NPO, notable positive SLP anomalies appear over mid-latitude North Pacific and northwestern part of North America, and marked negative SLP anomalies are seen over subtropical North Pacific with a center of action around 30° N, 160° W. Figure 2b shows regression map of rainfall anomalies in SON(0) onto the normalized ND(-1) JFM(0) NPO index. Significant decrease in rainfall anomalies are apparent over most parts of eastern Australia (i.e. east of 130° E). This result is consistent with Song et al. (2016), indicating that rainfall in SON(0) over eastern parts of the Australia tends to be below (above) normal

when preceding winter NPO is in its positive (negative) phase. In addition, it should be mentioned that spatial pattern of the winter NPO-related rainfall anomalies in SON(0) over Australia bears a resemblance to the first EOF mode of rainfall anomalies in SON(0) over Australia (Fig. 1b). In particular, the pattern correlation coefficient between the winter NPO-related rainfall anomalies and the first EOF mode of SON(0) rainfall anomalies over Australia reaches 0.7. This suggests that winter NPO is an important factor for the variation of the dominant pattern of rainfall anomalies over Australia in SON(0). According to the spatial distribution of rainfall anomalies in Fig. 2b, we define an Australian rainfall index (ARI for short) as region-mean rainfall over eastern part of the Australia (e.g. east of 130° E). Slight change of the region employed to define the ARI does not affect the main results of this study. Figure 2c exhibits the standardized time series of

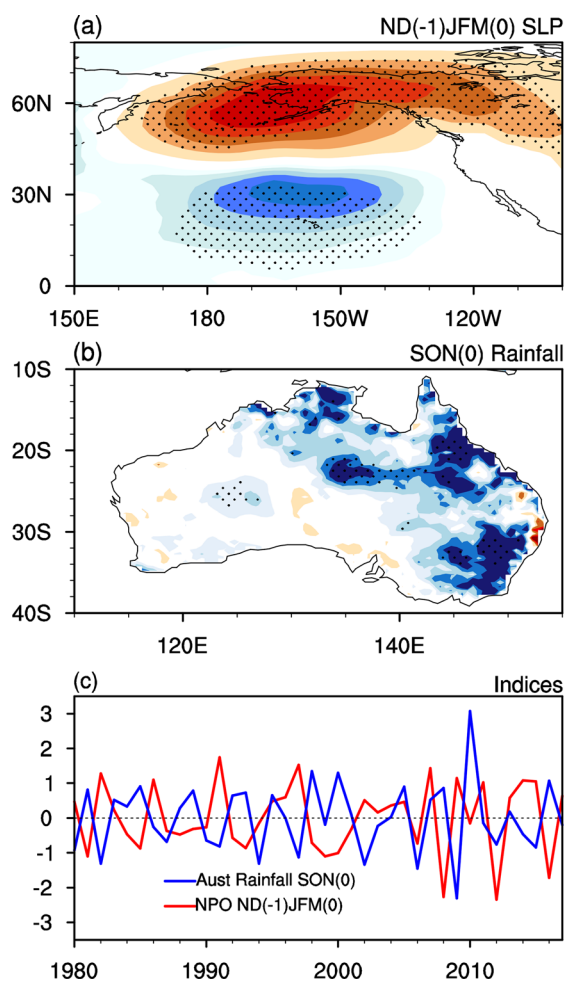


Fig. 2 **a** Winter (ND(-1)JFM(0)) SLP anomalies (unit: hPa) regressed upon the simultaneous winter NPO index over 1979–2016. **b** SON(0) Rainfall anomalies (unit: cm) regressed upon the ND(-1) JFM(0) NPO index over 1979–2016. Stippling regions in **a** and **b** indicate anomalies significant at the 95% confidence level. **c** Standardized time series of the ND(-1)JFM(0) NPO index and SON(0) Australian Rainfall index. Australian Rainfall index is defined as rainfall anomalies over the Australian region east of 130° E

the ND(-1)JFM(0) NPO index and the SON(0) ARI. The correlation coefficient between the two indices over 1979–2016 reaches -0.4 , significant at the 95% confidence level, further confirming that winter NPO index has a significant relationship with the rainfall anomalies over Australia during the following SON(0). In addition, it should be mentioned that the correlation coefficients between the autumn (SON(0)) Australian rainfall index and NPO index in MAM(0), JJA(0), and the simultaneous autumn (SON(0)) are -0.27 , -0.27 , and 0.04 , respectively. This suggests that the autumn Australian rainfall has a maximum correlation with the NPO index in preceding winter ($r = -0.4$). Hence, this study focuses on

investigating impact of NPO in preceding winter on the autumn Australian rainfall following Song et al. (2016).

The out-of-phase variation of the winter NPO index with the ARI in the following autumn is unstable. It has experienced a significant interdecadal weakening around the late-1990s, which can be clearly confirmed by the 19-year moving correlation correlations between the winter NPO index and the following autumn ARI (Fig. 3a). Using other lengths of moving correlation (e.g. 17-year and 21-year) can obtain very similar results (not shown). From Fig. 3a, winter NPO index has a significant negative correlation with the succedent autumn ARI before the late-1990s. However, their connection becomes weak and statistically insignificant after the late-1990s (Fig. 3a). Note that results derived from the three reanalysis datasets (i.e. NCEP-NCAR, ERA_Interim, and JRA55) are highly similar, all indicating that the relation between the winter NPO and autumn rainfall in the next year over eastern Australia underwent an obvious interdecadal change around the late-1990s (Fig. 3a). In the following, the whole analysis period of 1979–2016 is separated into two sub-periods (i.e. 1979–1997 and 1998–2016) both with 19-years for comparative analysis. The correlation coefficients between the winter NPO index and the subsequent autumn ARI are -0.67 and -0.25 during 1979–1997 and 1998–2016, respectively. The difference of the correlation coefficient between the two selected periods exceeds the 90% confidence level according to the Fisher's r-z transformation method, which is described in Sect. 2.

We further compare spatial distribution of rainfall anomalies over Australia in association with the preceding winter NPO index between 1979–1997 and 1998–2016. SON(0) rainfall anomalies over Australia regressed upon the ND(-1) JFM(0) NPO index during 1979–1997 and 1998–2016 are shown in Fig. 4a, b, respectively. As expected, there exists substantial difference in the SON(0) rainfall anomalies over Australia between the two periods. Before the late-1990s, pronounced decrease in rainfall appears in most part of eastern Australia (Fig. 4a). In addition, a small patch of significant positive rainfall anomalies appear over western Australia around 25° S and 120° E (Fig. 4a). By contrast, SON(0) rainfall anomalies over most portions of Australia are fairly weak during 1998–2016 (Fig. 4b). One may ask whether interdecadal change in the winter NPO-Australian autumn rainfall relation is related to change in the dominant mode of the Australian autumn rainfall anomalies? We have examined the dominant EOF mode of the Australian autumn rainfall anomalies during 1979–1997 and 1998–2016 (Fig. 1c, d). Results show that spatial pattern of the EOF1 of Australian autumn rainfall anomalies are similar during 1979–1997 (Fig. 1c) and 1998–2016 (Fig. 1d). Hence, the dominant mode of the Australian autumn rainfall anomalies does not undergo interdecadal change around the late-1990s.

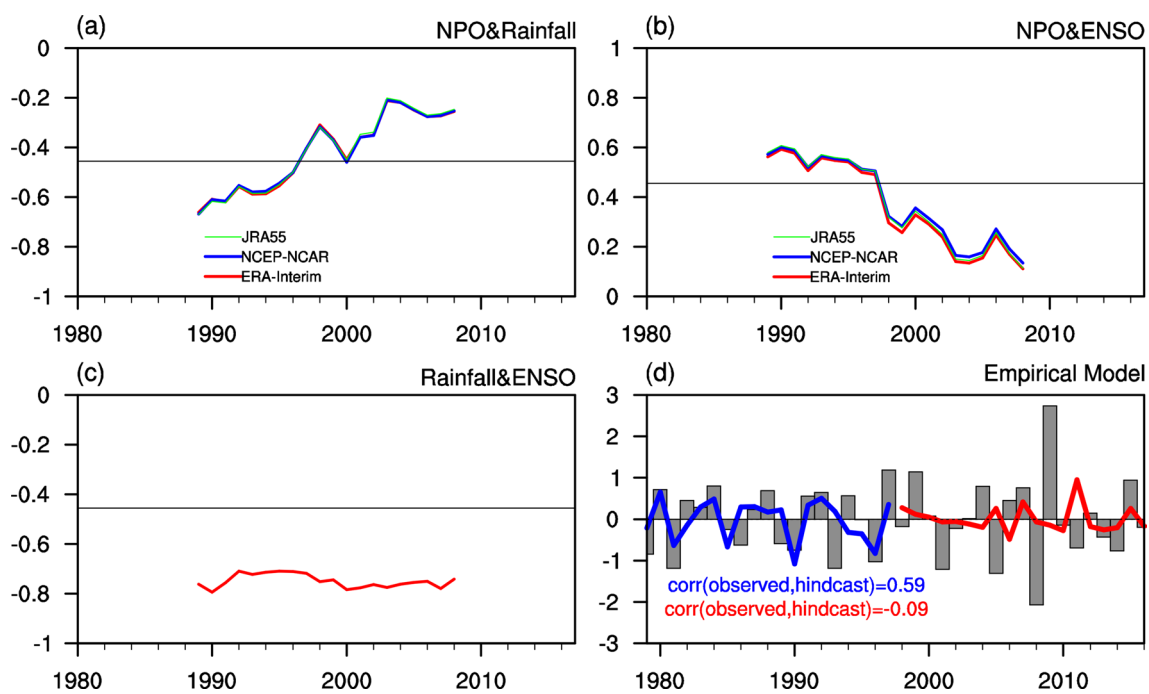


Fig. 3 **a** Moving correlation coefficients between ND(-1)JFM(0) NPO index and SON(0) Australian Rainfall index with a moving length of 19 years. **b** Moving correlation coefficients between ND(-1)JFM(0) NPO index and SON(0) Niño3.4 index with a moving length of 19 years. NPO indices are constructed based on the ERA-interim (red line), NCEP-NCAR (blue line), and JRA55 (green line) reanalysis datasets, respectively. **c** Moving correlation coefficients between SON(0) Australian Rainfall index and SON(0)

Niño3.4 index with a moving length of 19 years. Horizontal lines in **a–c** indicate the correlation coefficient significant at the 95% confidence level. **d** Observed time series of the SON(0) Australian Rainfall index (bar) over 1979–2016. The cross-validated hindcasts of the SON(0) Australian Rainfall index calculated by empirical model using the ND(-1)JFM(0) NPO index during 1979–1997 (blue curve) and 1998–2016 (red curve)

In view of the above interdecadal change of the influence of the winter NPO on the following autumn rainfall variation over eastern Australia, it is expected that the predictability of the SON(0) ARI based on the preceding ND(-1)JFM(0) NPO may also have changed around the late-1990s. Two empirical models are developed to predict the autumn ARI based on the preceding winter NPO index during 1979–1997 and 1998–2016, respectively. The following two equations correspond to the periods before and after the late-1990s, respectively, and are written as below:

$$\begin{aligned} \text{ARI}_{\text{em}}|_{\text{before}}(t) &= a_1 \times \text{NPO}(t) + b_1 \\ \text{and } \text{ARI}_{\text{em}}|_{\text{after}}(t) &= a_2 \times \text{NPO}(t) + b_2 \end{aligned}$$

here, $\text{ARI}_{\text{em}}|_{\text{before}}$ ($\text{ARI}_{\text{em}}|_{\text{after}}$) indicates ARI estimated by the empirical model during 1979–1997 (1998–2016). The hindcast skills of the empirical model are cross-validated via the leave-one-out scheme following previous studies (Chen et al. 2018b, 2019a, b). The leave-one-out scheme discards one year from the analysis period and estimates the regression coefficient based on the remaining data and then hindcasts the value of the discarded year. From Fig. 3d, it is obvious that when the winter NPO index is employed to hindcast the

ARI in the following autumn during 1979–1997, the cross validated correlation coefficient is 0.59, significant at the 99% confidence level. This suggests that winter NPO is an effective predictor for the prediction of the ARI in the following autumn. By contrast, during 1998–2016, when the winter NPO index is used to hindcast the succedent autumn ARI during 1998–2016, the cross validated correlation coefficient is very weak, with a value of only –0.09 (Fig. 3d). This indicates that after the late-1990s, using winter NPO to predict the autumn rainfall anomalies over Australia will lead to a false alarm.

In summary, above evidences suggest that impact of the winter NPO on the following autumn rainfall over eastern Australia has experienced a significant interdecadal change around the late-1990s. Before the late-1990s, impact of the winter NPO on the rainfall variation over eastern Australia in the following autumn is strong and significant, consistent with Song et al. (2016). During this period, winter NPO is an effective predictor for the prediction of the SON(0) rainfall over Australia. However, after the late-1990s, relation of the winter NPO with the following autumn Australian rainfall is very weak.

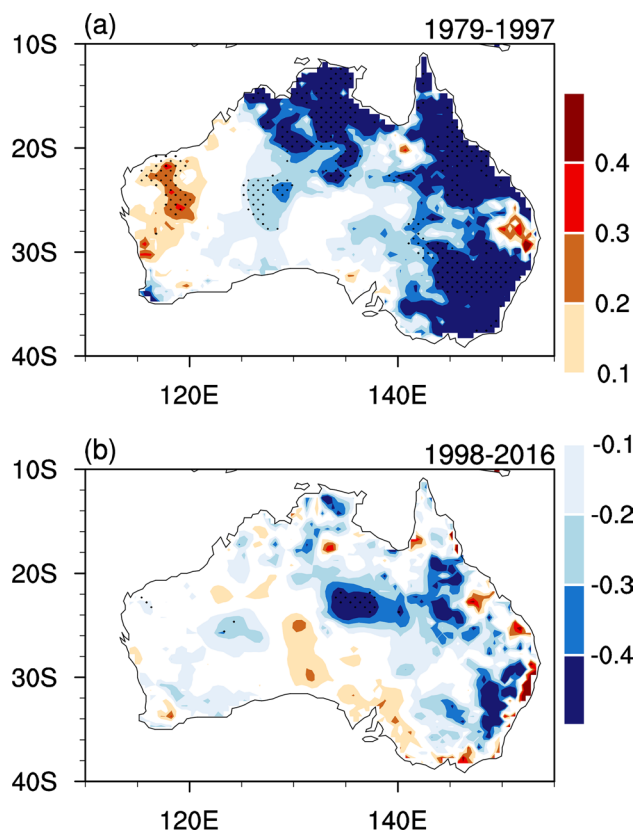


Fig. 4 SON(0) rainfall anomalies (unit: cm) regressed upon the standardized ND(-1)JFM(0) NPO index during **a** 1979–1997 and **b** 1998–2016, respectively. Stippling regions indicate rainfall anomalies significant at the 95% confidence level

4 Factors for the change of the relation between winter NPO and rainfall over Australia

In this section, we will examine the plausible factors contributing to interdecadal change of the winter NPO-autumn ARI relation around the late-1990s. Evolutions of SST and 850-hPa winds anomalies from ND(-1)JFM(0) to the following SON(0) associated with the ND(-1)JFM(0) NPO index during 1979–1997 and 1998–2016 are firstly examined and shown in Fig. 5. In addition, evolutions of precipitation anomalies related to the winter NPO index during the two periods are displayed in Fig. 6. For convenience of comparison, winds anomalies are also shown in Fig. 6. During 1979–1997, the physical processes for the impact of the winter NPO on the following autumn rainfall variation over eastern Australia are consistent with Song et al. (2016). Song et al. (2016) reported that positive winter NPO could lead to a significant El Niño-like warming in the tropical central and eastern Pacific in the following autumn. Then, the El Niño-like SST warming induced by the positive winter NPO contributes to decrease in the rainfall over Australia via

anomalous Walker circulation. In particular, positive phase of the winter NPO over 1979–1997, which is associated with a meridional atmospheric anomaly dipole over North Pacific, leads to formation of a tripolar SST anomaly pattern in the following spring (Fig. 5a) via modulation of the surface heat fluxes (will be discussed below), bearing several resemblances to that related to the Pacific meridional mode (Chiang and Vimont 2004; Zheng et al. 2021a) and Victoria mode (Ding et al. 2015, 2018). The tripolar SST anomaly pattern is associated with significant warm SST anomalies in the subtropical central North Pacific and mid-latitude North Pacific (around 40°–50° N), and cold SST anomalies in the subtropical western North Pacific and south China Sea (Fig. 5a). The subtropical central North Pacific warm SST anomalies are accompanied by enhanced atmospheric heating (indicated by significant positive precipitation anomalies) (Fig. 6b). The enhanced atmospheric heating, warm SST, and cyclonic anomalies over subtropical North Pacific maintain and extend southwestward to the tropical Pacific in the following summer via the positive wind-evaporation SST feedback process (Vimont et al. 2001, 2003a; Xie and Philander 1994; Song et al. 2016). Then, the strong westerly wind anomalies in the tropical western-central Pacific lead to an El Niño-like warming in the following autumn–winter via oceanic zonal advection process and through triggering eastward propagating Equatorial warm Kelvin waves, as has been demonstrated by many previous studies (Vimont et al. 2003a, b; Nakamura et al. 2006; Lengaigne et al. 2004; Chen et al. 2014, 2018a, 2020a; Zheng et al. 2021b). Previous study also indicated that positive winter NPO-related atmospheric circulation anomalies could contribute to formation of an El Niño-like warming in the following winter via the trade wind charging mechanism (Anderson and Perez 2015). In particular, the southwesterly wind anomalies over subtropical North Pacific related to the winter NPO (Fig. 5a) could provide anticyclonic wind stress curl anomalies near the tropical central Pacific (not shown). This would result in southward meridional Sverdrup transportation and lead to subsurface sea temperature warming over the tropical central Pacific (Fig. 7a). The subsurface temperature warming propagates upward and eastward, which contributes to positive SST anomalies in the tropical central-eastern Pacific in the following winter (Fig. 7c, e, g). Therefore, the trade wind charging process also has a contribution to the El Niño-like warming in the following winter generated by the preceding winter NPO during 1979–1997.

The El Niño-like SST warming in autumn in the tropical central and eastern Pacific generated by the preceding winter positive NPO induces an anomalous Walker circulation, with upward motion anomalies over the tropical central and eastern Pacific (indicated by convergent anomalies at the lower troposphere and divergent anomalies at the upper troposphere, Fig. 8a, c), and downward

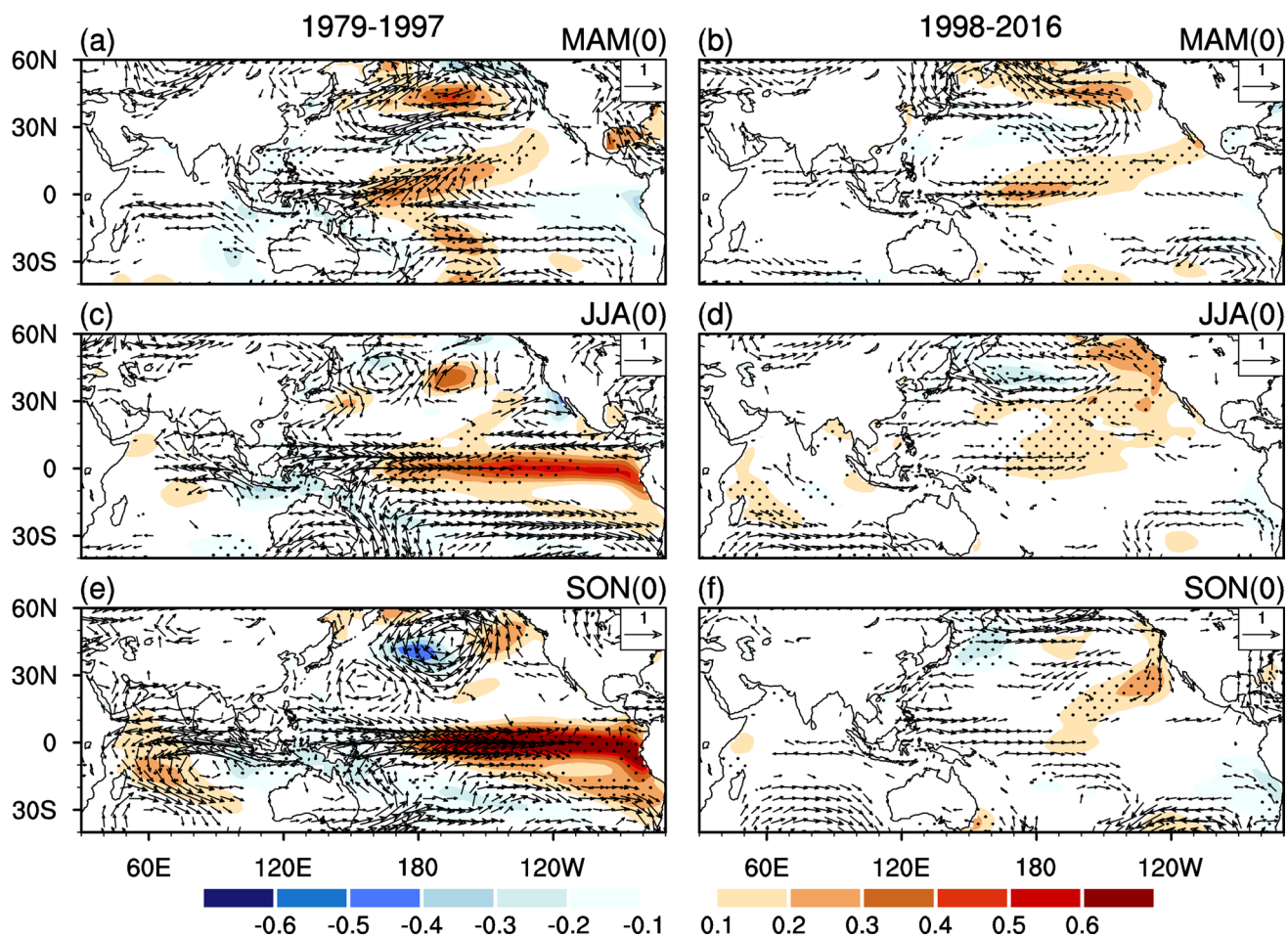


Fig. 5 Anomalies of SST (unit: $^{\circ}\text{C}$) and 850-hPa winds (unit: m s^{-1}) in **a**, **b** MAM(0), **c**, **d** JJA(0), **e**, **f** SON(0) regressed upon the ND(-1) JFM(0) NPO index during (left column) 1979–1997 and (right col-

umn) 1998–2016. Stippling regions in the figure indicate anomalies significant at the 95% confidence level

motion anomalies over tropical western Pacific including most parts of Australia (indicated by divergent anomalies at the lower troposphere and convergent anomalies at the upper troposphere, Fig. 8a, c). Finally, the anomalous downward motion leads to significant decrease in the rainfall over eastern Australia (Fig. 4a). The physical processes described above also apply to the negative phase of the winter NPO, but with opposite anomalies. It is noted that a positive IOD-like SST anomaly pattern also appears in the Indian Ocean, which is consistent with previous finding that a positive IOD event tends to appear following the development of El Niño events (Wang and Wang 2014). Studies have demonstrated that positive IOD event tends to lead to decrease in rainfall over most part of Australia via modulating atmospheric circulation (Ummenhofer et al. 2011). Hence, the accompanying IOD-like SST anomaly pattern related to the winter NPO may also contribute to decrease in the Australian autumn rainfall during 1979–1997.

However, for the period over 1998–2016, atmospheric circulation and SST anomalies over the tropical Pacific and associated subsurface temperature anomalies over equatorial Pacific related to the winter NPO are much weaker compared to those during 1979–1997. Thus, positive winter NPO could not lead to a clear El Niño-like SST warming in the tropical central and eastern Pacific (Figs. 5f, 6f). Accordingly, anomalous tropical Walker circulation is also weak (Fig. 8b, c). This explains why impact of the winter NPO on the rainfall over Australia in the following autumn is weak after the late-1990s. Moreover, we have examined the interdecadal change in the relation of the winter NPO with the ENSO in the following autumn (Fig. 4b). Time series of the moving correlation coefficient between the winter NPO index and the following autumn Niño-3.4 SST index (Fig. 3b) is highly similar to that of the moving correlation coefficient between the winter NPO and the autumn ARI, but with opposite signal (Fig. 3a). In particular, winter NPO has a significant correlation with the ENSO and rainfall variation over Australia

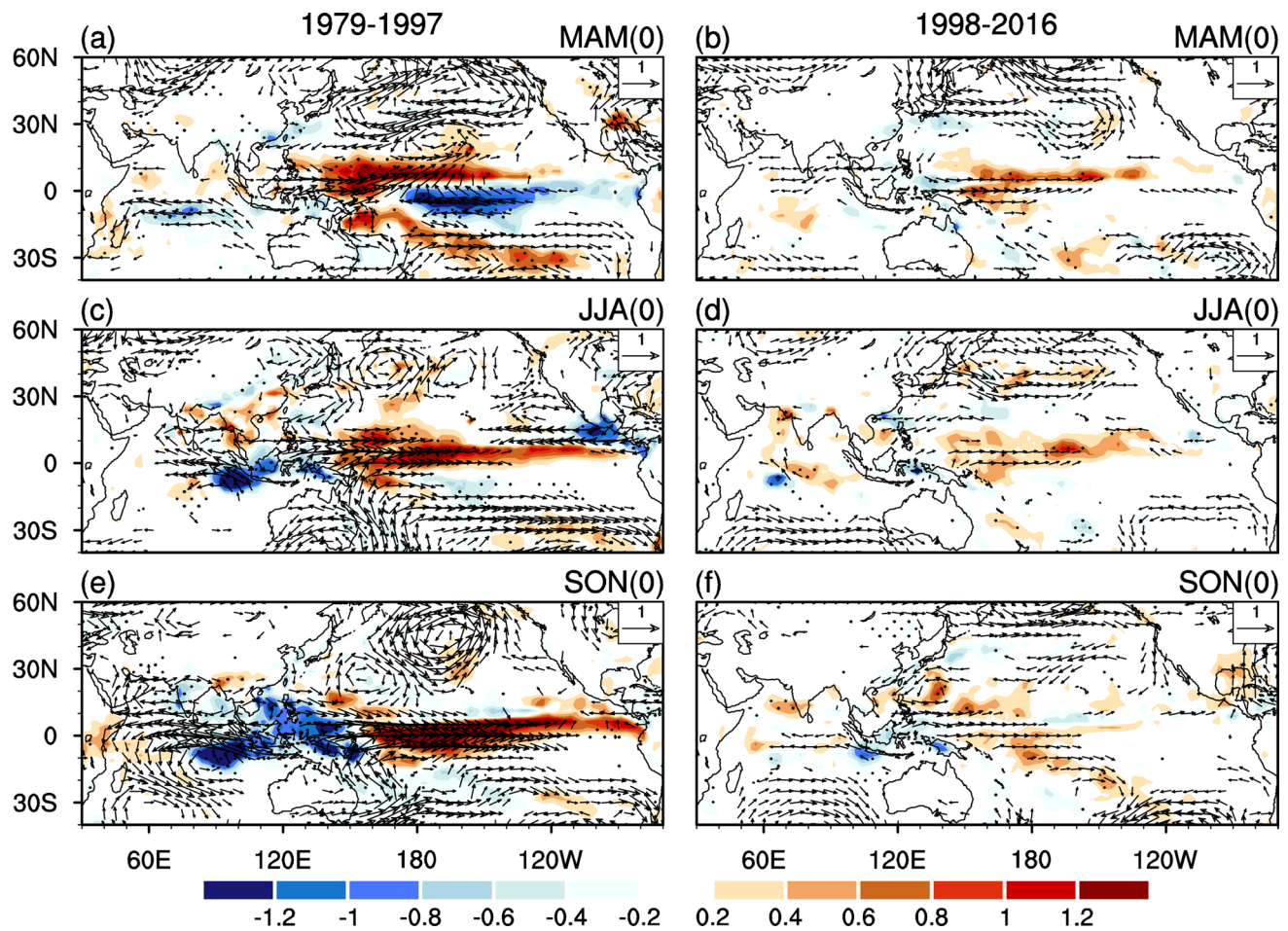


Fig. 6 Anomalies of precipitation (unit: mm day^{-1}) and 850-hPa winds (unit: m s^{-1}) in **a, b** MAM(0), **c, d** JJA(0), **e, f** SON(0) regressed upon the ND(-1)JFM(0) NPO index during (left column)

1979–1997 and (right column) 1998–2016. Stippling regions in the figure indicate anomalies significant at the 95% confidence level

during the following autumn before the late-1990s. However, after the late-1990s, impacts of the winter NPO on the following ENSO and rainfall over Australia are weak. Figure 3c shows 19-yr moving correlation of the SON(0) ARI and the SON(0) Niño3.4 index. It shows that ENSO has a stationary impact on the Australian rainfall (Fig. 3c). Above evidences suggest that interdecadal change in the connection of the winter NPO with the autumn rainfall over Australia is attributable to change in the impact of the winter NPO on the following tropical central and eastern Pacific SST.

Studies indicated that rainfall anomalies over Australia may also be partly related to change in the moisture transport (Ummenhofer et al. 2008; Sun et al. 2015). We have calculated the vertically integrated moisture flux and moisture divergence in SON(0) regressed upon the ND(-1)JFM(0) NPO index during 1979–1997 and 1998–2016, respectively (Fig. 9). During 1979–1997, eastward moisture advection appears over southeast Australia (Fig. 9a) that is reminiscent of the southwesterly wind anomalies at the low-level

troposphere (Fig. 5a). Strong moisture divergence anomalies are seen over tropical western Pacific (Fig. 9a), corresponding to strong negative precipitation there (Fig. 6a). In addition, significant moisture divergence anomalies with weaker amplitude are observed between 20 and 30° S along 145° E, contributing to decrease in rainfall there. Moisture convergence anomalies are seen over Australian east coast around 25–30° S and south coast around 140° E (Fig. 9a), which cannot explain decrease in rainfall there. During 1998–2016, westward moisture advection and moisture convergence anomalies are seen over Australian eastern coast, which are favorable for increase in rainfall there. In general, above analysis indicates that moisture transport may not be the main factors responsible for differences in rainfall anomalies over Australia related to the winter NPO during the two periods.

Above analyses have indicated that change in the relation of winter NPO with the Australian rainfall is mainly due to the unstable impact of the winter NPO on the following

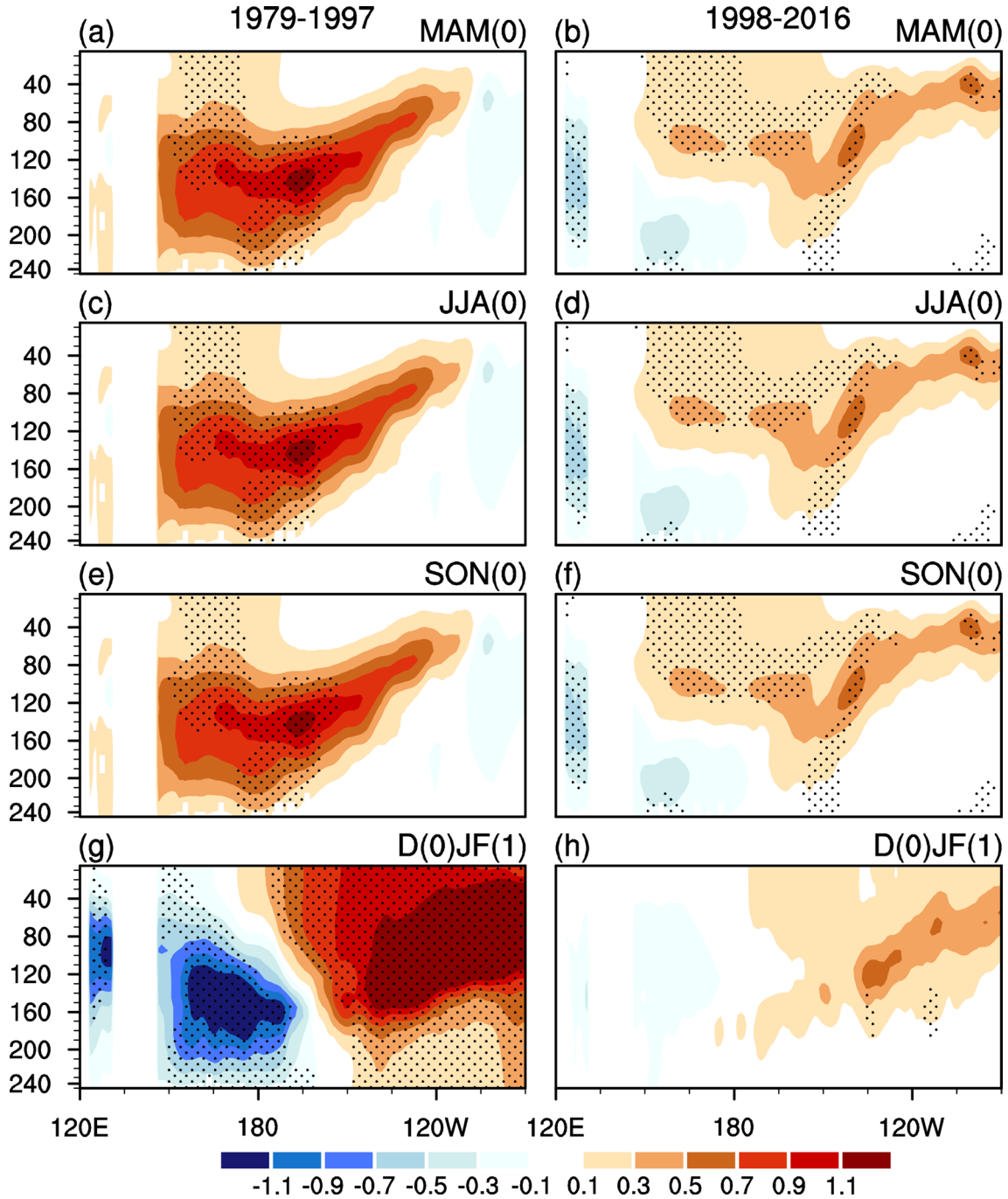


Fig. 7 Subsurface temperature anomalies (unit: $^{\circ}\text{C}$) in the tropical Pacific (5°S – 5°N -average) in **a**, **b** MAM(0), **c**, **d** JJA(0), **e**, **f** SON(0), and **g**, **h** D(0)JF(1) related to the winter NPO index during

(left) 1979–1997 and (right) 1998–2016, respectively. Stippling regions indicate anomalies significant at the 95% confidence level

ENSO. A question needs to be further addressed is: what are the plausible factors responsible for changes in the impact of the winter NPO on the following ENSO? Fig. 5a, b indicate that North Pacific is dominated by a tripolar SST anomaly pattern in spring during the two periods, but with a slight northward shift for the period after the late-1990s. In addition, amplitude of the SST warming in the tropical

and central North Pacific is larger before than after the late-1990s (Fig. 5a, b). In particular, values of SST anomalies more than $0.2 \text{ } ^{\circ}\text{C}$ cover much larger area over the subtropical North Pacific during 1979–1997 compared to those during 1998–2016. The larger SST warming over the subtropical North Pacific contributes to stronger positive precipitation anomalies and results in stronger westerly wind anomalies

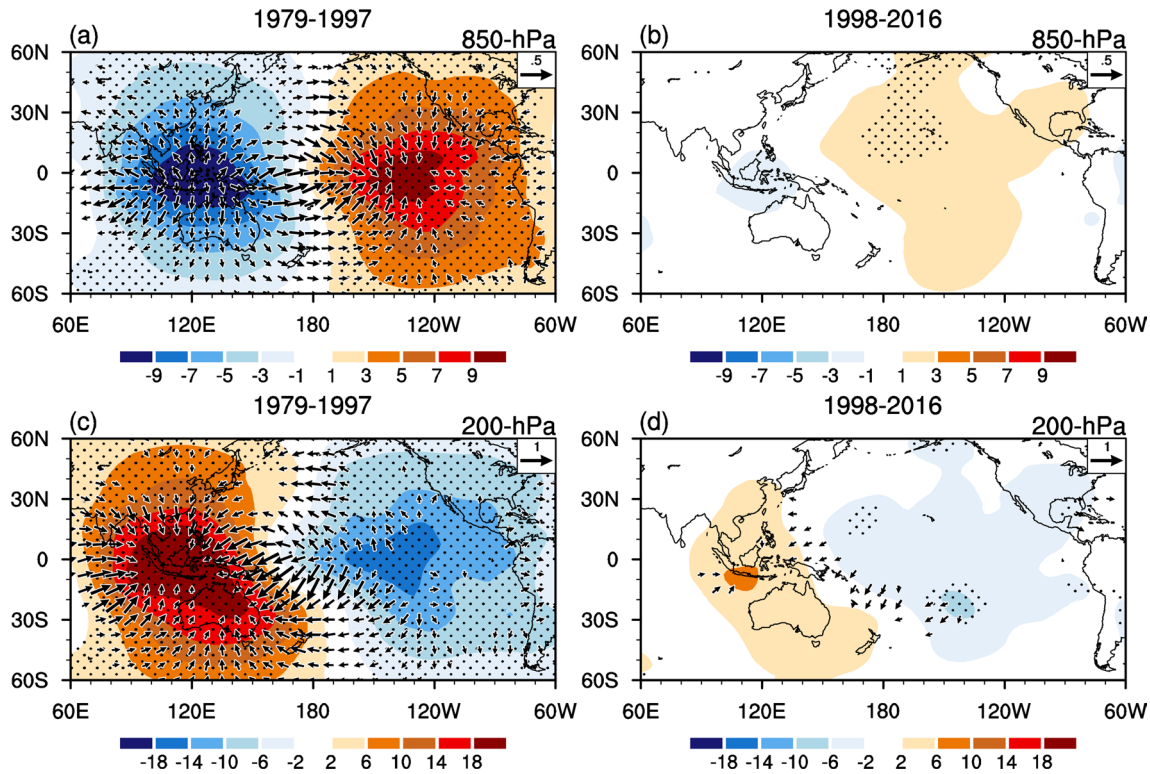


Fig. 8 Anomalies of velocity potential (shadings; unit: $10^5 \text{ m}^2 \text{ s}^{-1}$) and divergent winds (vectors; unit: m s^{-1}) at **a, b** 850-hPa and **c, d** 200-hPa in SON(0) regressed upon the standardized NDJFM(0) NPO

index during (left column) 1979–1997 and (right column) 1998–2016. Stippling regions indicate velocity potential anomalies significant at the 95% confidence level

over the tropical western-central Pacific via the wind-evaporation-SST feedback process, which finally contributes to a more significant El Niño-like warming in the tropical central-eastern Pacific before the late-1990s.

Previous studies have demonstrated that winter NPO-related atmospheric circulation anomalies lead to a tripolar SST anomaly pattern in the following spring mainly via modulating the surface heat fluxes (dominated by surface latent heat fluxes) (Vimont et al. 2001, 2003a, b; Alexander et al. 2010; Chen et al. 2013). Hence, we firstly examine differences in the spatial structure of the winter NPO to explain the differences in the distribution of the spring SST anomalies in the North Pacific. Figure 10a, b show winter SLP anomalies regressed upon the simultaneous winter NPO index during 1979–1997 and 1998–2016, respectively. The winter NPO is featured by a meridional dipolar pattern over North Pacific both for the two periods, with positive SLP and anticyclonic anomalies over mid-latitude and negative SLP and cyclonic anomalies over subtropical North Pacific during its positive phase (Fig. 10a, b). The southeasterly wind anomalies over subtropical North Pacific oppose the climatological northeasterly winds and contribute to SST warming there (Fig. 5a, b) via reduction of the surface net heat fluxes. In addition, the anomalous easterly winds over mid-latitude North Pacific would lead to decrease in the climatological

westerly wind speeds and also result in warm SST anomalies there. By contrast, the northeasterly wind anomalies over the subtropical North Pacific contribute to cold SST anomalies via bringing colder air from higher latitudes, which enhance the surface evaporation. Above processes explain formation of the spring tripolar SST anomaly pattern over the North Pacific in association with the preceding winter NPO, which have been demonstrated by previous studies using observations and numerical experiments (Vimont et al. 2001, 2003a, b). However, a comparison of Fig. 10a, b indicates that the wintertime NPO-related meridional dipolar atmospheric anomaly over North Pacific is located more northeastward for the period after than before the late-1990s. In particular, center of the negative SLP anomalies over subtropical North Pacific is located around 30° N during 1998–2016. By contrast, during 1979–1997, center of the maximum SLP anomalies appears around 25° N . Figure 10c, d compare the winter surface turbulent heat flux anomalies regressed upon the simultaneous winter NPO index during 1979–1997 and 1998–2016. Here, surface turbulent heat flux is the sum of surface latent and sensible heat fluxes. In addition, in this study, values of the surface heat flux are positive (negative) when their directions are downward (upward), which contribute to warm (cold) SST anomalies. During 1979–1997, significant and positive surface turbulent heat flux anomalies

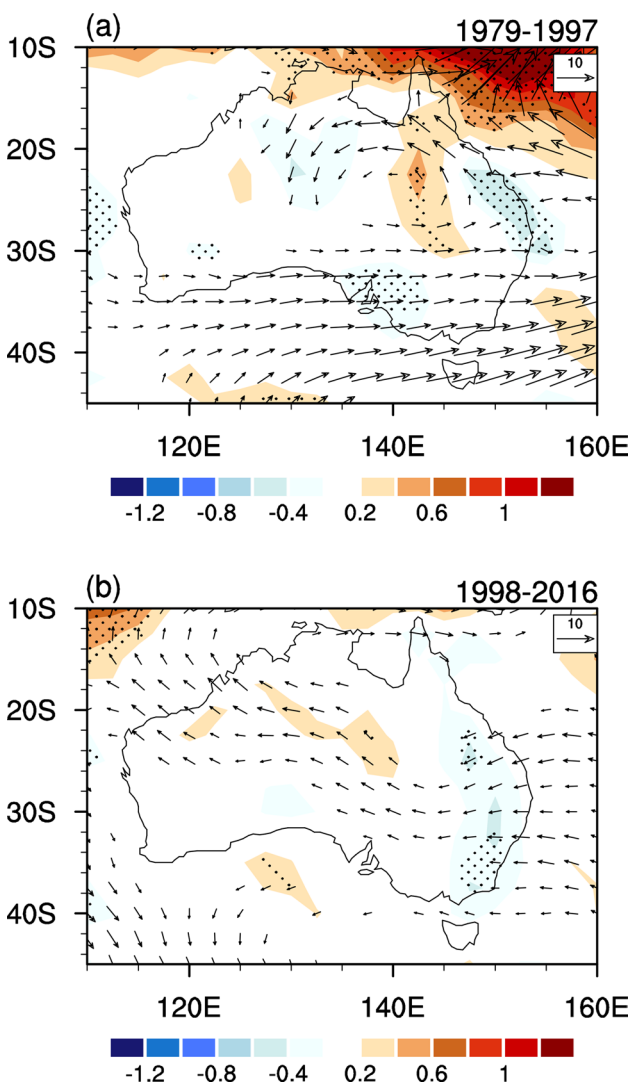


Fig. 9 Vertically integrated (1000 hPa–400 hPa) moisture flux (vectors, unit: $\text{kg m}^{-1} \text{ s}^{-1}$) and moisture divergence ($10^{-5} \text{ kg m}^{-2} \text{ s}^{-1}$) in SON(0) regressed upon the ND(-1)JFM(0) NPO index during **a** 1979–1997 and **b** 1998–2016, respectively. Stippling regions indicate moisture divergence anomalies significant at the 95% confidence level

are seen in the tropical and subtropical North Pacific in winter (Fig. 10c), which contribute to formation of warm SST anomalies there in the following spring (Fig. 5a). By contrast, positive surface turbulent heat flux anomalies over subtropical North Pacific are much weaker and shift more northward during 1998–2016 (Fig. 10d) compared to those during 1979–1997 (Fig. 10c), consistent with the northward shifted spatial structure of the winter NPO-related atmospheric circulation anomalies (Fig. 10a, b), which explain the weaker warm SST anomalies over the tropical and subtropical North Pacific after the late-1990s (Fig. 5a, b). Above evidences suggest that difference in the spatial structure of the winter NPO leads to difference in the spring SST anomalies over the North Pacific, which alter the air-sea interaction

over the tropical and subtropical North Pacific and modulate the winter NPO-ENSO relation.

We further examine the factors leading to change in the spatial structure of the winter NPO. It is well accepted that winter NPO is an important atmospheric intrinsic mode (Wallace and Gutzler 1981; Rogers 1981; Lau 1988; Linkin and Nigam 2008). Variation of the NPO represents meridional movement of the jet stream over extratropical North Pacific. In addition, the interaction between the mean flow and synoptic-scale eddy (also called storm track activity) plays a crucial role in the formation and maintenance of the winter NPO (Lau 1988; Linkin and Nigam 2008). Specifically, during positive phase of the winter NPO, easterly wind anomalies over the mid-latitude North Pacific (Fig. 11a, b) are accompanied by decrease in the storm track activity (Fig. 11c, d) (Lau 1988). As has been demonstrated by previous studies (Lau 1988; Cai et al. 2007; Chen et al. 2014, 2020a, b), decrease in the storm track activity over mid-latitude would immediately contribute to anticyclonic vorticity forcings to its north and cyclonic vorticity forcings to its south, which in turn maintain the meridional dipolar atmospheric anomaly related to the winter NPO. Hence, change in the meridional locations of the climatological jet stream and storm track activity over North Pacific would have an impact on the spatial structure of the winter NPO.

Figure 12a, b show differences in the climatological 200-hPa zonal wind and storm track between 1979–1997 and 1998–2016. For convenience of comparison, the climatology of zonal wind and storm track are also shown in Fig. 12, which are indicated by the contours. It shows that the maximum climatological zonal winds appear to the south of Japan around 35° N with a value larger than 55 m s^{-1} . By comparison, climatological zonal winds south (north) of 35° N over North Pacific during 1979–1997 are significant larger (weaker) than those during the 1998–2016. This indicates that jet stream over North Pacific shifts southward before the late-1990s compared to the period after the late-1990s. Changes in the North Pacific storm track activity (Fig. 12b) are consistent with the jet stream (Fig. 12a). In particular, maximum center of the climatological storm track is observed over mid-latitude North Pacific (Fig. 12b). During 1979–1997, storm track activities over North Pacific to the south of the climatological center are significantly stronger than those during 1998–2016, indicating a southward shift of the climatological storm track. Hence, difference in the meridional location of the climatological jet stream and storm track explains change in the spatial structure of the winter NPO between the two periods before and after the late-1990s. Specifically, a northward movement of the meridional structure of the winter NPO after the late-1990s is attributed to the associated northward shifted climatological jet stream and storm track activity.

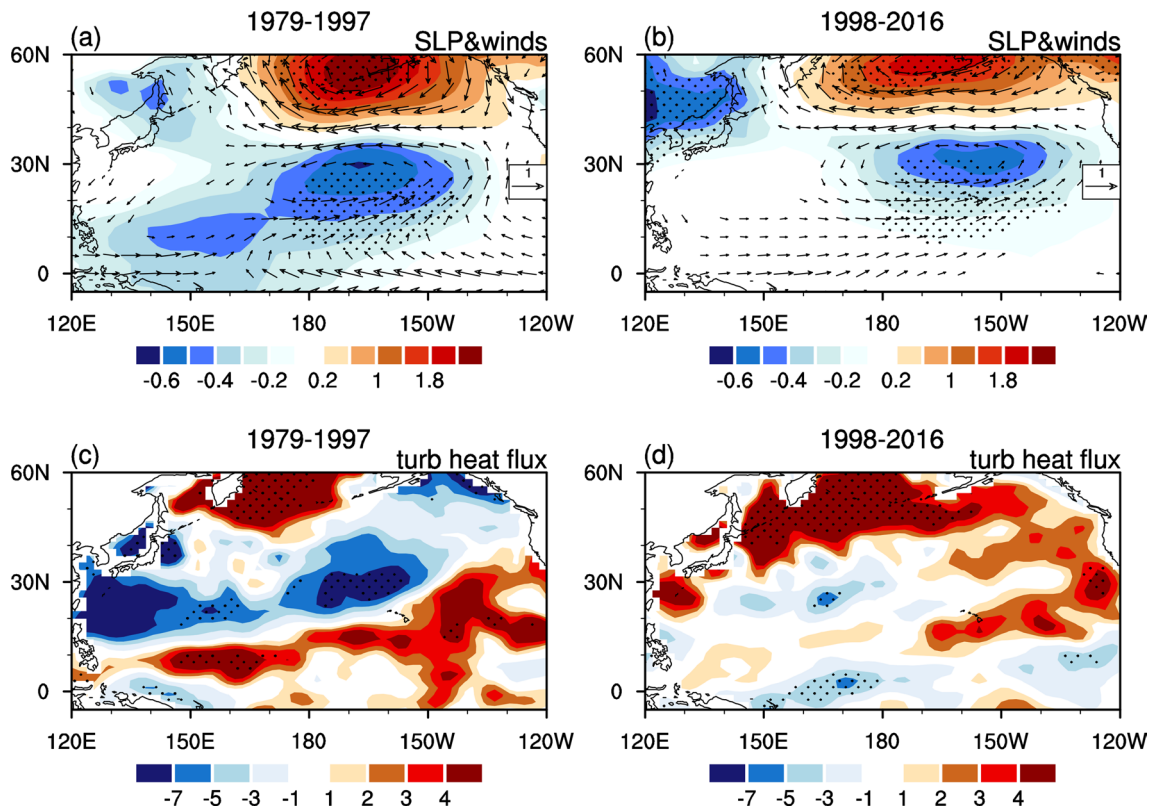


Fig. 10 Anomalies of **a, b** SLP (shadings; unit: hPa) and 850-hPa winds (vectors, unit: m s^{-1}), and **c, d** surface turbulent heat fluxes (unit: W m^{-2}) in ND(-1)JFM(0) regressed upon the ND(-1)JFM(0) NPO index during **a, b** 1979–1997 and **c, d** 1998–2016. Surface tur-

bulent heat flux is the sum of surface latent and sensible heat fluxes. Stippling regions in **a, b** and **c, d** indicate SLP and turbulent heat flux anomalies significant at the 95% confidence level

5 Possible role of the AMO in the modulation of the winter NPO-autumn ARI relation

It is known that AMO has a shift from its negative to positive phase around the late-1990s (Kerr 2000; Enfield et al. 2001; Park and Li 2019). In addition, studies have reported that AMO has a significant modulation effect on the climatological jet stream and storm track activity over North Pacific (Zhang and Delworth 2007; Peings and Magnusdottir 2014; Sun et al. 2017; Chen et al. 2019a, b, 2020b). In particular, North Pacific jet stream and storm track activity are stronger and located more southward during negative than positive AMO phases. Above evidences motivate us to examine an interesting issue: whether the winter NPO-following autumn ARI relation is modulated by the AMO? To address this issue, we compare the AMO index (Fig. 13b) with the moving correlation coefficient between the winter NPO index and following autumn ARI over period of 1948–2016 (Fig. 13a). Here, the winter NPO index is calculated based on the SLP data from the NCEP-NCAR reanalysis. From Fig. 13b, AMO is in its positive phase before the early-1990s and after the

late-1990s. Negative phase of the AMO is seen from the early-1990s to the late-1990s. Moving correlation results indicate that winter NPO has a significant negative correlation with the following ARI from the early-1990s to the late-1990s, corresponding to the negative phase of the AMO. By contrast, the relationship between the winter NPO and the succedent autumn ARI is weak and statistically insignificant before the early-1990s and after the late-1990s, which corresponding well to the positive phase of the AMO. The correlation coefficient between the winter NPO index and following autumn ARI during negative phase of the AMO (a total of 30 years) reaches -0.63 , significant at the 99% confidence level. However, the correlation is -0.29 during the positive phase of AMO (a total of 38 years), cannot pass the 90% confidence level. Here, positive (negative) phase of the AMO is defined when the normalized AMO index is larger (less) than zero. Above evidences suggest that the AMO indeed has a notable modulation effect on the relationship between the winter NPO and the following autumn rainfall variation over Australia. That is to say, AMO acts as an important modulator for the relation of the winter NPO with rainfall variation over Australia in the following autumn.

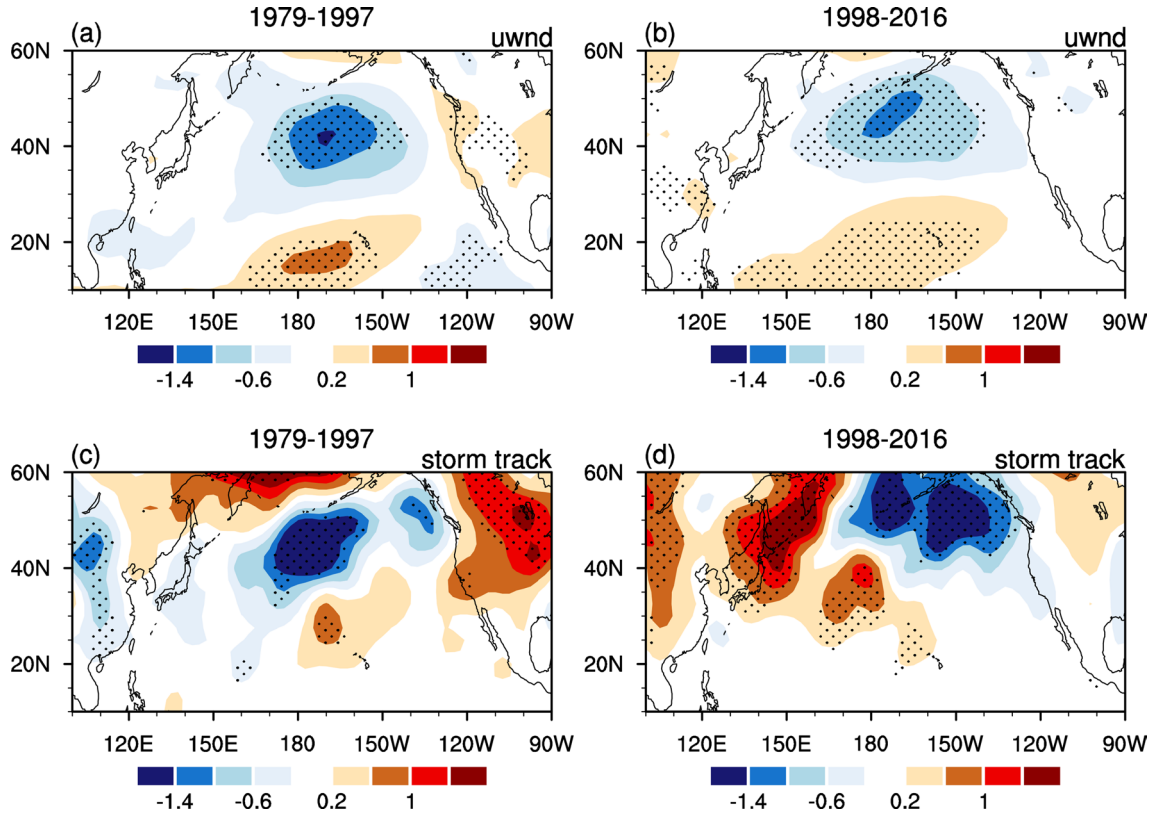


Fig. 11 Anomalies of 850-hPa a, b zonal winds (unit: m s^{-1}) and c, d storm track (unit: m) in ND(-1)JFM(0) regressed upon the ND(-1) JFM(0) NPO index during (left column) 1979–1997 and (right col-

umn) 1998–2016. Stippling regions indicate anomalies significant at the 95% confidence level

Figure 14 shows SON(0) SST and rainfall anomalies regressed upon the preceding ND(-1)JFM(0) NPO index during positive and negative phases of the AMO. It is clear that during negative AMO phase, positive winter NPO can induce a significant El Niño-like SST warming in the tropical central and eastern Pacific in the following autumn (Fig. 14b), and lead to significant decrease in rainfall over most parts of Australia (Fig. 14d). By contrast, influence of the winter NPO on the following autumn ENSO and rainfall variation over Australia are weak during the positive phase of the AMO. This suggests that AMO modulates the winter NPO-subsequent autumn Australian rainfall relation via modulating the relation between the winter NPO and ENSO. Furthermore, we have examined evolutions of SST, atmospheric circulation and precipitation anomalies over Pacific from ND(-1)JFM(0) to SON(0) during positive and negative phases of the AMO (not shown). These results (not shown) are similar to those shown in Figs. 5 and 6. Namely, the meridional dipolar atmospheric anomaly pattern over North Pacific in winter related to the NPO is located more southward during the negative than positive AMO phases. As a result, SST warming and accompanied positive precipitation anomalies in the tropical and subtropical central

North Pacific are stronger during the negative AMO phase. As such, winter NPO can exert a stronger impact on the following ENSO during negative AMO phase.

Figure 15 shows differences in the 200-hPa zonal winds and storm track activity (indicated by shadings) between negative and positive phases of the AMO. It is obvious that zonal winds and storm track activity are significantly stronger during negative than positive phases of the AMO over the regions to the southeast of the climatological centers of the zonal winds and storm track (Fig. 15). This suggests that North Pacific storm track and jet stream shift more southward during negative AMO phase, consistent with previous findings (Zhang and Delworth 2007; Peings and Magnusdottir 2014; Sun et al. 2017). These results indicate that AMO could modulate the spatial structure of the winter NPO via modulating the mean state of atmospheric circulation and storm track activity over North Pacific. Differences in the spatial structure of the winter NPO further lead to distinct impact of the NPO on the following ENSO and rainfall over Australia via positive air-sea interaction processes.

In addition, previous studies have reported that SST anomalies in the mid-high latitudes Southern Ocean at multi-decadal timescale have a significant out-of-phase relation with the

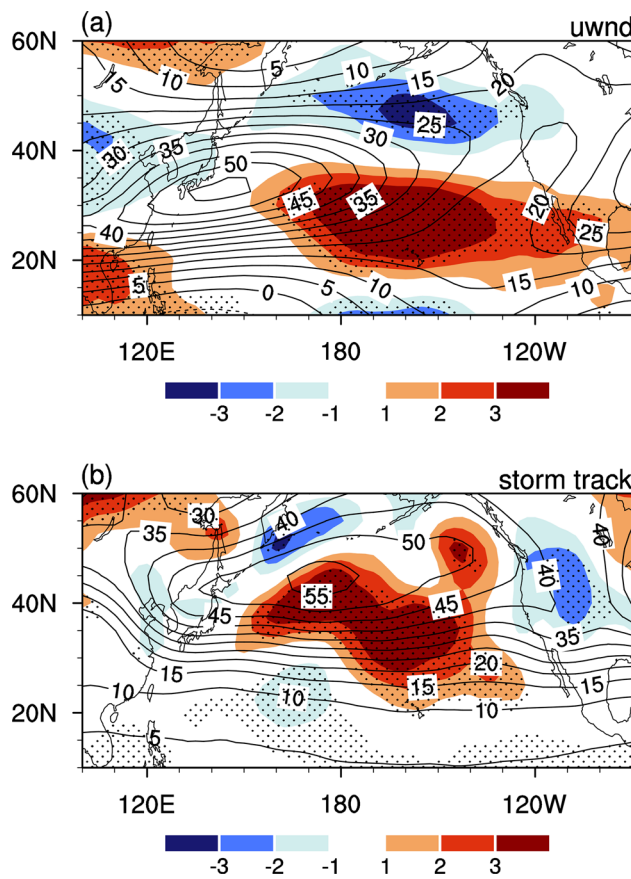


Fig. 12 Climatological distributions of a 200-hPa zonal winds (contours; unit: m s^{-1}) and b storm track (contours; unit: m) over the period of 1979–2016. Differences in the climatology of a 200-hPa zonal winds (shadings; unit: m s^{-1}) and b storm track (shadings, unit: m) between periods of 1979–1997 and 1998–2016 (former minus latter). Stippling regions indicate the differences that are significantly different from zero at the 95% confidence level

AMO (Sun et al. 2013, 2015). In particular, positive (negative) AMO phase is generally corresponding to a significant SST cooling (warming) in the mid-high latitudes Southern Ocean, which increases (decreases) the meridional temperature gradient and subtropical westerlies (Sun et al. 2013, 2015). These extratropical mean state changes of SST and mean flow may provide a favorable condition for the activity of extratropical disturbance and thus may exert impact on the Australian rainfall via modulating the subtropical moist transport (Sun et al. 2013, 2015). Hence, this may also provide a possible pathway for the impact of the AMO on the winter NPO-Australian rainfall relation.

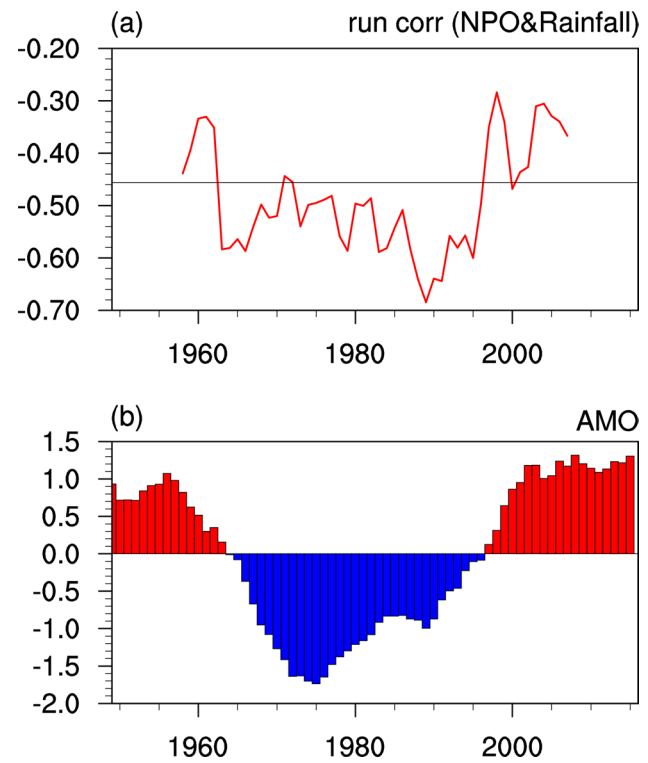


Fig. 13 a Moving correlation coefficients between ND(-1)JFM(0) NPO index and SON(0) Australian Rainfall index with a moving length of 19 years during 1948–2017. Horizontal line in a indicates the correlation coefficient significant at the 95% confidence level. b Smoothed AMO index during 1950–2017

6 Summary

Previous study indicated that wintertime NPO has a strong impact on the rainfall variation over eastern Australia in the following autumn. The present study reveals that the impact of the winter NPO on the following autumn rainfall over eastern Australia shows a significant interdecadal weakening around the late-1990s based on multiple observations and reanalysis datasets. After the late-1990s, the relation between winter NPO and subsequent autumn rainfall over eastern Australia is weak and insignificant. We find that wintertime NPO can (not) be considered as an effective predictor for the prediction of the autumn Australian rainfall before (after) the late-1990s. This study further examines the factors leading to the interdecadal weakening of the connection, which is summarized in Fig. 16.

This study finds that the wintertime meridional atmospheric anomaly pattern, with anticyclonic anomaly over mid-latitudes and cyclonic anomaly over subtropical North Pacific during positive phase of the winter NPO, is located more southward before the late-1990s compared to that after the late-1990s (Fig. 16a, b). Before the late-1990s, the winter NPO-related atmospheric circulation anomalies

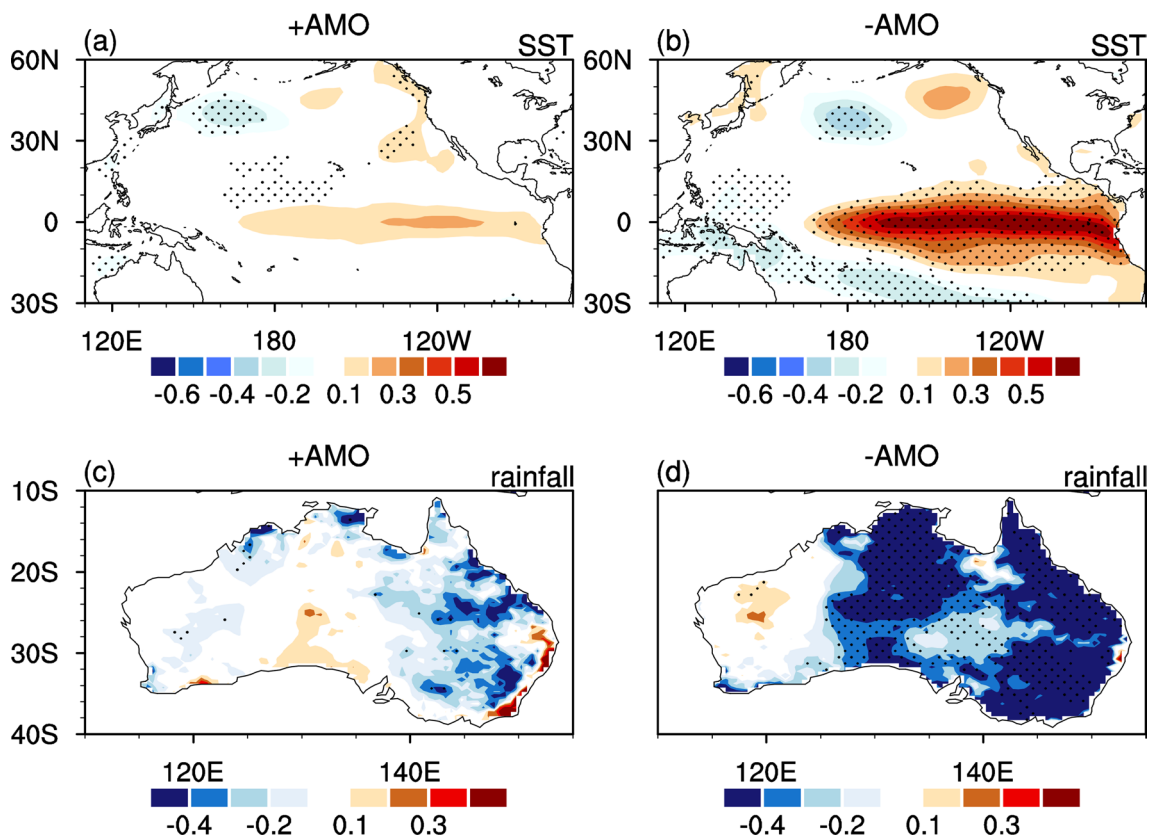


Fig. 14 Anomalies of **a, b** SST (unit: $^{\circ}\text{C}$) and **c, d** Rainfall (unit: mm day^{-1}) in SON(0) regressed upon the ND(-1)JFM(0) NPO index during (left column) positive and (right column) negative phases of AMO. Stippling regions indicate anomalies significant at the 95% confidence level

lead to formation of a significant tripolar SST anomaly pattern in the following spring via modulating the surface net heat fluxes (Fig. 16a). The associated SST warming in the subtropical North Pacific leads to enhanced atmospheric heating, which could induce an anomalous cyclone over the subtropical western North Pacific via a Rossby wave type atmospheric response (Fig. 16a). The SST warming, the increase in atmospheric heating, and the cyclonic anomaly over subtropical North Pacific maintain and extend southwestward to the tropical central Pacific in the following summer via wind-evaporation-SST feedback mechanism. Then, the westerly wind anomalies over the tropical western-central Pacific contribute to formation of El Niño-like SST anomaly pattern in the following autumn–winter. Finally, the autumn El Niño-like SST warming would induce an anomalous Walker circulation in the tropics with anomalous upward motion in the tropical eastern Pacific and anomalous downward motion in the tropical western Pacific and most parts of eastern Australia, which lead to decrease in the rainfall there (Fig. 16a).

However, after the late-1990s, the NPO-related atmospheric circulation anomalies over the North Pacific shift northward (Fig. 16b). In addition, the associated SST

warming and positive precipitation anomalies over the subtropical North Pacific are weaker compared to those before the late-1990s (Fig. 16b). As such, wintertime NPO cannot induce clear westerly wind anomalies over the tropical western-central Pacific, and thus cannot result in significant SST warming in the tropical central-eastern Pacific in the following autumn–winter. Correspondingly, winter NPO cannot exert clear impact on the following autumn rainfall variation over eastern Australia. Further analysis indicates that change in the meridional location of the wintertime NPO-related atmospheric circulation is attributable to change in the meridional locations of the climatological jet stream and storm track activity over North Pacific. In particular, centers of the extratropical North Pacific jet stream and storm track activity are located more southward before than after the late-1990s.

We note that interdecadal change in the relationship between the winter NPO and following autumn Australian rainfall around the late-1990s is also related to the phase shift of the AMO. Using a longer time series, it is confirmed that AMO indeed has a significant modulation on the winter NPO-subsequent autumn Australian rainfall relation. Climatology of the North Pacific jet stream and

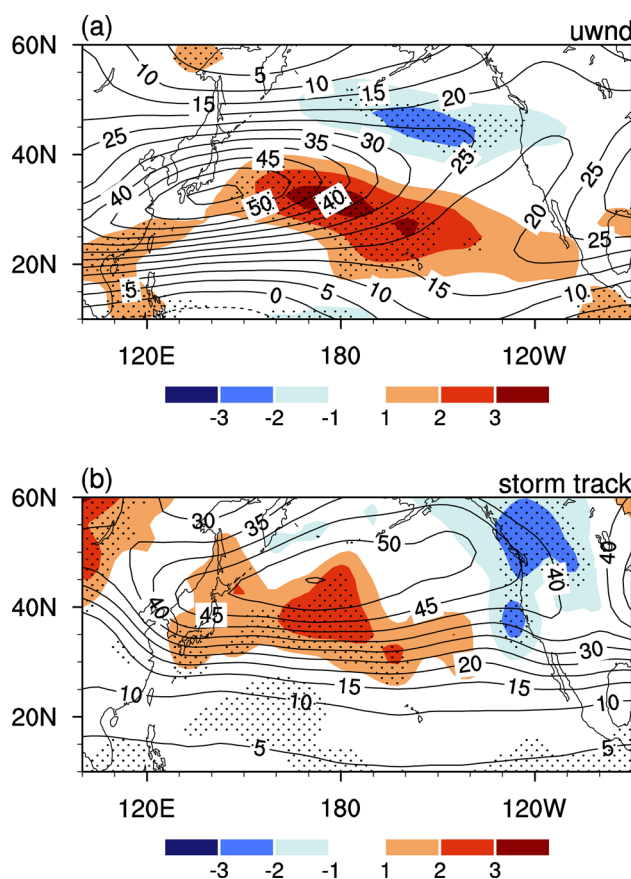


Fig. 15 Climatological distributions of **a** 200-hPa zonal winds (contours; unit: m s^{-1}) and **b** storm track (contours; unit: m). Differences in the climatology of **a** 200-hPa zonal winds (shadings; unit: m s^{-1}) and **b** storm track (shadings, unit: m) between negative and positive phases of AMO. Stippling regions indicate the differences between negative and positive phases of AMO that are significantly different from zero at the 95% confidence level

storm track and NPO-related meridional dipolar atmospheric anomaly pattern are located more southward during negative than positive AMO phases (Fig. 16a, b). As such, SST warming and positive precipitation anomalies over the subtropical North Pacific and westerly wind anomalies over the tropical western-central Pacific in the following spring, and SST warming in the tropical central-eastern Pacific in the following autumn are much stronger during negative than positive AMO phases (Fig. 16a, b). Hence, winter NPO has a strong (weak) impact on the Australian rainfall during the negative (strong) AMO phase.

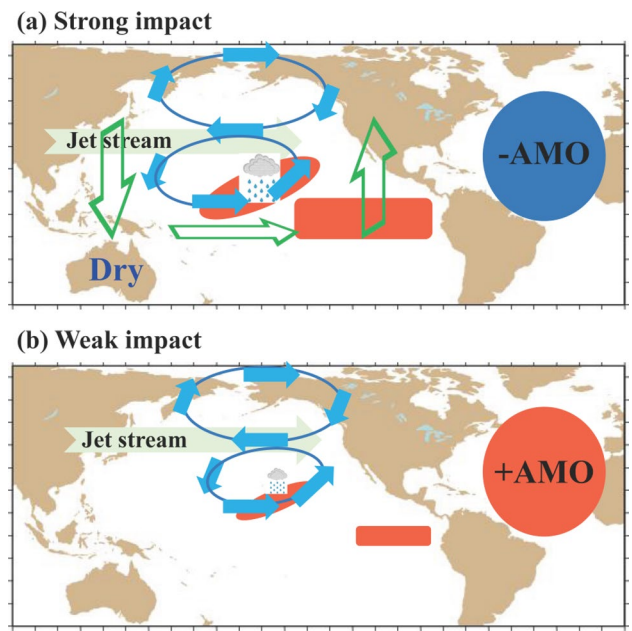


Fig. 16 Schematic diagram showing the physical processes responsible for the change in the impact of the winter NPO on the following Autumn rainfall variation over Australia. Blue (red) shadings indicate cold and warm SST anomalies. Blue vectors indicate wind anomalies related to the winter NPO. Green vectors indicate the anomalous tropical walker circulation anomalies induced by the warm SST anomalies in the tropical central and eastern Pacific

Acknowledgements We thank three anonymous reviewers for their constructive suggestions and comments, which help to improve the paper. This work was supported jointly by the National Natural Science Foundation of China (Grants 41721004 and 41961144025), and the Chinese Academy of Sciences Key Research Program of Frontier Sciences (QYZDY-SSW-DQC024).

Author contributions LYS and SFC designed the research, performed the analysis, and wrote the manuscript. All authors revised the paper, discussed the results and commented on the manuscript.

Data availability NCEP-NCAR data is obtained from <ftp://ftp.cdc.noaa.gov/Datasets/>. ERA-Interim data is obtained from <https://www.ecmwf.int/en/forecasts/datasets/reanalysis-datasets/era-interim>. JRA55 data are derived from <https://rda.ucar.edu/datasets/ds628.1/>. ERSSTv5 data is derived from <https://www.esrl.noaa.gov/psd/data/gridded/>. UDEL precipitation data is derived from https://www.esrl.noaa.gov/psd/data/gridded/data.UDel_AirT_Precip.html. GPCP data is obtained from <http://www.esrl.noaa.gov/psd/data/gridded/data.gpcp.html>. AMO index is derived from <https://www.esrl.noaa.gov/psd/data/timeseries/AMO/>.

Code availability (software application or custom code) Figures in this study are constructed with the NCAR Command Language (<http://www.ncl.ucar.edu/>). All codes used in this study are available from the corresponding author (S.C.).

Declarations

Conflict of interest The authors declare no potential conflicts of interest.

References

- Adler RF, Huffman GJ, Chang A, Ferraro R, Xie P, Janowiak J, Rudolf B, Schneider U, Curtis S, Bolvin D, Gruber A, Susskind J, Arkin P, Nelkin E (2003) The version 2 global precipitation climatology project (GPCP) monthly precipitation analysis (1979–present). *J Hydrometeorol* 4:1147–1167
- Alexander MA, Vimont DJ, Chang P, Scott JD (2010) The impact of extratropical atmospheric variability on ENSO: testing the seasonal footprinting mechanism using coupled model experiments. *J Clim* 23:2885–2901
- Allan RJ (1988) El Niño southern oscillation influences in the Australian region. *Prog Phys Geogr* 12:313–348
- Anderson BT, Perez RC (2015) ENSO and non-ENSO induced charging and discharging of the equatorial Pacific. *Clim Dyn* 45:2309–2327
- Ashok K, Guan ZY, Yamagata T (2003) Influence of the Indian Ocean dipole on the Australian winter rainfall. *Geophys Res Lett* 30(15):1821
- BOM (2006) Statement on drought for the 3, 6, and 10-month periods ending 31 October 2006—drought intensifies over eastern and southern Australia as spring rains fail. Drought Statements (National Climate Centre, Bureau of Meteorology), 3 Nov 2006.
- Bretherton CS, Widmann M, Dymnikov VP, Wallace JM, Bladé I (1999) The effective number of spatial degrees of freedom of atime-varying field. *J Clim* 12:1990–2009
- Cai WJ, Cowan T (2009) La Niña Modoki impacts Australia autumn rainfall variability. *Geophys Res Lett* 36:L12805
- Cai M, Yang S, Van den Dool H, Kousky V (2007) Dynamical implications of the orientation of atmospheric eddies: a local energetics perspective. *Tellus* 59A:127–140. <https://doi.org/10.1111/j.1600-0870.2006.00213.x>
- Cai WJ, Cowan T, Raupach M (2009) Positive Indian Ocean Dipole events precondition southeast Australia bushfires. *Geophys Res Lett*. <https://doi.org/10.1029/2009GL039902>
- Cai WJ, van Rens P, Cowan T, Sullivan A (2010) Asymmetry in ENSO teleconnection with regional rainfall, its multidecadal variability, and impact. *J Clim* 23:4944–4955
- Catto J, Nicholls N, Jakob C (2012) North Australian sea surface temperatures and the El Niño-Southern Oscillation in observations and models. *J Clim* 25:5011–5029
- Chen SF, Chen W, Yu B, Graf H (2013) Modulation of the seasonal footprinting mechanism by the boreal spring Arctic Oscillation. *Geophys Res Lett* 40:6384–6389
- Chen SF, Yu B, Chen W (2014) An analysis on the physical process of the influence of AO on ENSO. *Clim Dyn* 42(3–4):973–989
- Chen SF, Wu R, Song LY, Chen W (2018a) Combined influence of the Arctic Oscillation and the Scandinavia pattern on spring surface air temperature variations over Eurasia. *J Geophys Res Atmos* 123:9410–9429
- Chen SF, Yu B, Chen W, Wu R (2018b) A review of atmosphere-ocean forcings outside the tropical Pacific on the El Niño-Southern Oscillation occurrence. *Atmosphere* 9:439
- Chen SF, Wu R, Song LY, Chen W (2019a) Interannual variability of surface air temperature over mid-high latitudes of Eurasia during boreal autumn. *Clim Dyn* 53:1805–1821
- Chen SF, Song LY, Chen W (2019b) Interdecadal modulation of AMO on the winter North Pacific Oscillation—following winter ENSO relationship. *Adv Atmos Sci* 36(12):1393–1403. <https://doi.org/10.1007/s00376-019-9090-1>
- Chen SF, Wu R, Chen W, Yu B (2020a) Recent weakening of the linkage between the spring Arctic Oscillation and the following winter El Niño-Southern Oscillation. *Clim Dyn* 54(1):53–67
- Chen SF, Chen W, Wu R, Song L (2020b) Impacts of the Atlantic Multidecadal Oscillation on the relationship of the Spring Arctic Oscillation and the following East Asian summer monsoon. *J Clim* 33:6651–6672
- Chiang JC, Vimont DJ (2004) Analogous Pacific and Atlantic meridional modes of tropical atmosphere-ocean variability. *J Clim* 17:4143–4158
- Chiew FHS, Piechota TC, Dracup JA, McMahon TA (1998) El Niño/Southern Oscillation and Australian rainfall, streamflow and drought: links and potential for forecasting. *J Hydrol* 204(1):138–149
- Dee DP, Uppala SM, Simmons AJ et al (2011) The ERA-Interim reanalysis: configuration and performance of the data assimilation systems. *Q J R Meteorol Soc* 137:553–597. <https://doi.org/10.1002/qj.828>
- Ding RQ, Li JP, Tseng YH, Sun C, Guo Y (2015) The Victoria mode in the North Pacific linking extratropical sea level pressure variations to ENSO. *J Geophys Res Atmos* 120:27–45
- Ding RQ, Li J, Tseng YH, Li L, Sun C, Xie F (2018) Influences of the North Pacific Victoria mode on the South China Sea summer monsoon. *Atmosphere* 9:229
- Dou J, Wu ZW (2018) Southern Hemisphere origins for interannual variations of Tibetan Plateau snow cover in boreal summer. *J Clim* 31:7701–7718
- Dou J, Wu ZW, Zhou Y (2017) Potential impact of the May Southern Hemisphere annular mode on the Indian summer monsoon rainfall. *Clim Dyn* 49:1257–1269
- Dou J, Wu ZW, Li J (2020) The strengthened relationship between the Yangtze River Valley summer rainfall and the Southern Hemisphere annular mode in recent decades. *Clim Dyn* 54:1607–1624
- Duchon CE (1979) Lanczos filtering in one and two dimensions. *J Appl Meteorol* 18:1016–1022
- Ebita A, Kobayashi S, Ota Y et al (2011) The Japanese 55-year reanalysis “JRA-55”: an interim report. *Sci Online Lett Atmos Sola* 7:149–152. <https://doi.org/10.2151/sola.2011-038>
- Enfield DB, Mestas-Nunez AM, Trimble PJ (2001) The Atlantic multidecadal oscillation and its relation to rainfall and river flows in the continental U.S. *Geophys Res Lett* 28:2077–2080. <https://doi.org/10.1029/2000GL012745>
- Gallant AJE, Hennessy KJ, Risbey J (2007) Trends in rainfall indices for six Australian regions: 1910–2005. *Aust Meteorol Mag* 56(4):233–239
- Hendon HH, Thompson DWJ, Wheeler MC (2007) Australian rainfall and surface temperature variations associated with the Southern Hemisphere annular mode. *J Clim* 20:2452–2467
- Huang B et al (2017) Extended Reconstructed Sea Surface Temperature version 5 (ERSSTv5): upgrades, validations, and intercomparisons. *J Clim* 30:8179–8205
- Kalnay E et al (1996) The NCEP/NCAR 40-Year Reanalysis Project. *Bull Am Meteorol Soc* 77:437–471
- Kerr RA (2000) A North Atlantic climate pacemaker for the centuries. *Science* 288:1984–1985. <https://doi.org/10.1126/science.288.5473.1984>
- Lau NC (1988) Variability of the observed midlatitude storm tracks in relation to low-frequency changes in the circulation pattern. *J Atmos Sci* 45:2718–2743
- Lengaigne M, Guilyardi E, Boulanger JP, Menkes C, Delecluse P, Inness CJ, Slingo J (2004) Triggering of El Niño by westerly wind events in a coupled general circulation model. *Clim Dyn* 23:601–620

- Linkin ME, Nigam S (2008) The north pacific oscillation-west Pacific teleconnection pattern: mature-phase structure and winter impacts. *J Clim* 21:1979–1997
- Lu L, Hedley D (2004) The impact of the 2002–03 drought on the economy and agricultural employment. Economic Roundup Autumn 2004, The Treasury, Australian Government, 25–44. http://www.treasury.gov.au/documents/817/PDF/roundup_autumn_2004.pdf
- Matsuura K, Willmott CJ (2009) Terrestrial air temperature: 1900–2008 gridded monthly time series (version 5.01). University of Delaware. http://www.esrl.noaa.gov/psd/data/gridded/data.UDel_AirT_Precip.html
- Nakamura T, Tachibana Y, Honda M, Yamane S (2006) Influence of the Northern Hemisphere annular mode on ENSO by modulating westerly wind bursts. *Geophys Res Lett* 33:L07709. <https://doi.org/10.1029/2005GL025432>
- Nicholls N (1984a) Seasonal relationships between Australian rainfall and north Australian sea surface temperature. Extended Abstracts, Conf. on Australian Rainfall Variability, Arkaroola. Australian Academy of Science, pp 71–73.
- Nicholls N (1984b) The Southern Oscillation, sea-surface-temperature, and interannual fluctuations in Australian tropical cyclone activity. *J Climatol* 4:661–670
- Nicholls N (2010) Local and remote causes of the southern Australian autumn-winter rainfall decline, 1958–2007. *Clim Dyn* 34:835–845
- Park J, Li T (2019) Interdecadal modulation of El Niño–tropical North Atlantic teleconnection by the Atlantic multidecadal oscillation. *Clim Dyn* 52:5345–5360
- Peings Y, Magnusdottir G (2014) Forcing of the wintertime atmospheric circulation by the multidecadal fluctuations of the North Atlantic Ocean. *Environ Res Lett* 9:034018. <https://doi.org/10.1088/1748-9326/9/3/034018>
- Rogers JC (1981) The North Pacific Oscillation. *J Climatol* 1:39–57
- Ropelewski CF, Halpert MS (1987) Global and regional scale precipitation patterns associated with the El Niño/Southern Oscillation. *Mon Weather Rev* 115:1606–1626
- Saji NH, Goswami BN, Vinayachandran PN, Yamagata T (1999) A dipole mode in the tropical Indian Ocean. *Nature* 401:360–363
- Song L, Li Y, Duan W (2016) The influence of boreal winter extratropical North Pacific Oscillation on Australian spring rainfall. *Clim Dyn* 47:1181–1196
- Sun C, Li JP, Jin FF, Ding RQ (2013) Sea surface temperature interhemispheric dipole and its relation to tropical precipitation. *Environ Res Lett* 8:044006
- Sun C, Li JP, Feng J, Xie F (2015) A decadal-scale teleconnection between the North Atlantic Oscillation and subtropical eastern Australian rainfall. *J Clim* 28:1074–1092
- Sun C, Kucharski F, Li JP, Jin FF, Kang IS, Ding RQ (2017) Western tropical Pacific multidecadal variability forced by the Atlantic multidecadal oscillation. *Nat Commun* 8:15998
- Taschetto AS, England MH (2009) El Niño Modoki impacts on Australian rainfall. *J Clim* 22(11):3167–3174
- Ummenhofer CC, Sen Gupta A, Pook MJ, England MH (2008) Anomalous rainfall over southwest Western Australia forced by Indian Ocean sea surface temperatures. *J Clim* 21:5113–5134
- Ummenhofer CC, Sen Gupta A et al (2011) Indian and Pacific Ocean influences on southeast Australian drought and soil moisture. *J Clim* 24(5):1313–1336
- Vimont DJ, Battisti DS, Hirst AC (2001) Footprinting: a seasonal connection between the tropics and mid-latitudes. *Geophys Res Lett* 28:3923–3926
- Vimont DJ, Battisti DS, Hirst AC (2003a) The seasonal footprinting mechanism in the CSIRO general circulation models. *J Clim* 16:2653–2667
- Vimont DJ, Wallace JM, Battisti DS (2003b) The seasonal footprinting mechanism in the Pacific: implications for ENSO. *J Clim* 16:2668–2675
- Walker GT, Bliss EW (1932) World weather V. Mem R Meteorol Soc 4:53
- Wallace J, Gutzler D (1981) Teleconnections in the geopotential height field during the Northern Hemisphere winter. *Mon Weather Rev* 109:784–812
- Wang G, Hendon HH (2007) Sensitivity of Australian rainfall to inter-El Niño variations. *J Clim* 20(16):4211–4226
- Wang X, Wang CZ (2014) Different impacts of various El Niño events on the Indian Ocean Dipole. *Clim Dyn* 42:991–1005
- Wu ZW, Li J, Wang B, Liu X (2009) Can the Southern Hemisphere annular mode affect China winter monsoon? *J Geophys Res* 114:D11107
- Wu ZW, Dou J, Lin H (2015) Potential influence of the November–December Southern Hemisphere annular mode on the East Asian Winter precipitation: a new mechanism. *Clim Dyn* 44:1215–1226
- Xie SP, Philander SGH (1994) A coupled ocean-atmosphere model of relevance to the ITCZ in the eastern Pacific. *Tellus A* 46:340–350
- Yeh SW, Yi DW, Sung MK, Kim YH (2018) An eastward shift of the North Pacific Oscillation after the mid-1990s and its relationship with ENSO. *Geophys Res Lett* 45:6654–6660
- Yu JY, Lu MM, Kim ST (2012) A change in the relationship between tropical central Pacific SST variability and the extratropical atmosphere around 1990. *Environ Res Lett* 7:034025
- Zhang R, Delworth TL (2007) Impact of the Atlantic multidecadal oscillation on North Pacific climate variability. *Geophys Res Lett* 34:L23708
- Zhao W, Chen SF, Chen W, Yao S, Nath D, Yu B (2019a) Interannual variations of the rainy season withdrawal of the monsoon transitional zone in China. *Clim Dyn* 53:2031–2046
- Zhao W, Chen W, Chen SF, Yao S, Nath D (2019b) Interannual variations of precipitation over the monsoon transitional zone in China during August–September: role of sea surface temperature anomalies over the tropical Pacific and North Atlantic. *Atmos Sci Lett* 20:E872
- Zhao W, Chen W, Chen SF, Yao S, Nath D (2020) Combined impact of tropical central-eastern Pacific and North Atlantic sea surface temperature on precipitation variation in monsoon transitional zone over China during August–September. *Int J Climatol* 40:1316–1327
- Zheng YQ, Chen W, Chen SF, Yao SL, Cheng CL (2021a) Asymmetric impact of the boreal spring Pacific Meridional Mode on the following winter El Niño-Southern Oscillation. *Int J Climatol* 41:3525–3538
- Zheng YQ, Chen SF, Chen W, Yu B (2021b) Diverse influences of spring Arctic Oscillation on the following winter El Niño-Southern Oscillation in CMIP5 models. *Clim Dyn* 56:275–297
- Zhu YL, Wang HJ (2010) The relationship between the Aleutian Low and the Australian summer monsoon at interannual time scales. *Adv Atmos Sci* 27:177–184

Publisher's Note Springer Nature remains neutral with regard to jurisdictional claims in published maps and institutional affiliations.